Natural Compounds Targeting Human Histamine H_1 Receptor For Anti-Allergic Therapy

A Thesis

Submitted in partial fulfillment of the requirements for the award of the degree of

Master of Technology

In

Biotechnology

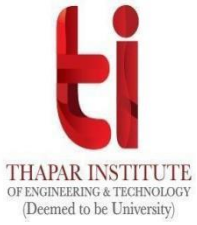

Submitted By

Shivangi Jain

(Reg no. 602204017)

Under the Supervision of

Dr Atul Kumar Upadhyay

Assistant Professor

Department of Biotechnology

Thapar Institute of Engineering and Technology, Patiala, 147004, Punjab

July 2024

CERTIFICATE

This is to certify that the thesis entitled, "**Natural compounds targeting human histamine H_1 receptor for anti-allergic therapy**" being submitted by Shivangi Jain (Reg. No. 602204017), in partial fulfilment of the requirements for the award of the degree of **Master of Technology** in **Biotechnology**, **Thapar Institute of Engineering and Technology, Patiala, Punjab** is a bonafide work carried out under the guidance and conception of **Dr Atul Kumar Upadhya,** Assistant Professor, Department of Biotechnology and that no part of this thesis has been submitted for the award of any other degree.

Date: 30/07/2024

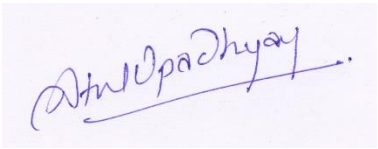

Dr Atul Kumar Upadhyay

Assistant Professor

Department of Biotechnology,

Thapar Institute of Engineering and Technology,

Patiala, Punjab

DECLARATION

I hereby certify that the work, which is being presented in the thesis, entitled **Natural compounds targeting Human Histamine H_1 Receptor for Anti-Allergic Therapy**, in partial fulfillment of the requirements for the award of the degree of **Master of Technology** and submitted to the institution is an authentic record of my own work carried out during the period **August 2023** to **June 2024** under the supervision **of Dr Atul Kumar Upadhyay, Assistant Professor, Department of Biotechnology, Thapar Institute of Engineering and Technology, Patiala, Punjab, India**. I have also cited the references of the text(s) from where they have been taken.

The matter presented in this thesis has not been submitted elsewhere for the award of any other degree or diploma from any institution.

Date: 30/07/2024

Shivangi Jain

602204017

This is to certify that the above statement made by the candidate is correct to the best of my knowledge.

Date: 30/07/2024

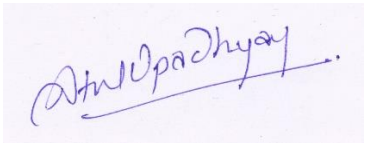

Dr Atul Kumar Upadhyay

ACKNOWLEDGEMENTS

I want to express my deepest gratitude to My Supervisor, **Dr Atul Kumar Upadhyay, Assistant Professor, Department of Biotechnology.** I am immensely grateful for his invaluable guidance, expertise, and encouragement throughout my dissertation course. His insightful feedback and constant support have helped shape the direction and quality of this thesis. This thesis would not have been possible without his unfailing support and belief in me. Working under the supervision of **Dr Atul Kumar Upadhyay** was a privilege.

I would like to extend my appreciation to **Dr M.S. Reddy, Head, Department of Biotechnology, Thapar Institute of Engineering and Technology, Patiala, Punjab,** for allowing me to do this project work. The academic and administrative support offered by the university has been pivotal in facilitating a conducive research environment. I appreciate all faculty members' assistance, motivation, and spiritual support throughout my M.Tech. in Biotechnology.

I am indebted to **Ms. Tanmayee Basu** and **Ms. Rashi Chugh** for their assistance and collaboration during the experimental phases of this study. I am immensely grateful for their dedication, expertise, and support, has significantly contributed to the execution and success of my experiments. Their willingness to share knowledge, troubleshoot issues, and provide hands-on assistance has been crucial in overcoming challenges and obtaining accurate and reliable results. I would like to extend my sincere thanks to **Ms. Arashdeep Kour** and **Ms. Tarushree Gupta** for their unwavering support and belief in me.

I am grateful to my parents, **Mr. Jatinder Jain** and **Mrs. Pooja Jain**, for their love, encouragement, and understanding throughout this challenging academic endeavor. Their constant support and belief in my abilities have motivated and strengthened me.

I regard this opportunity as a significant turning point in my professional progress. I will work diligently to use the knowledge and abilities I have acquired to achieve my career objective.

Shivangi Jain

INDEX

LIST OF TABLES

LIST OF FIGURES

ABSTRACT

Background: Allergies, exacerbated by environmental degradation, have a global impact and can pose life-threatening dangers in severe cases. Food allergies, which are an integral part of the "second wave" of the allergy epidemic, can be either IgE or non-IgE mediated. They result in symptoms that affect multiple systems in the body and have a significant impact on millions of people. Earlier antihistamines, such as doxepin, resulted in notable drowsiness and central nervous system (CNS) complications. In response, subsequent antihistamines like cetirizine were created to alleviate these problems, but encountered difficulties nonetheless. The current research is primarily centered around the *In-Silico* studies with include virtual screening, molecular docking and MD simulation of new natural anti-allergic compounds targeting the human H1 receptor to improve the compatibility and effectiveness of drugs.

Results: This in silico study predicts novel natural compounds, silymarin and kenusanone A, as potential antihistamine agents targeting the human histamine H_1 receptor. Through a comprehensive virtual screening involving ADMET evaluation, molecular docking, and molecular dynamic simulations, these compounds demonstrated significant binding affinity, stability, and favorable physicochemical properties. The reduced binding free energy and stable protein-ligand interactions suggest their efficacy in inhibiting allergic reactions with minimized side effects. The findings offer valuable insights for the development of safer and more effective antihistamine drugs, leveraging the therapeutic potential of natural compounds.

Keywords: Anti Allergic compounds, virtual screening, histamine receptors, DFT, molecular docking, ADMET and PAINS analysis, MMPBSA, molecular dynamic simulation

GRAPHICAL ABSTRACT

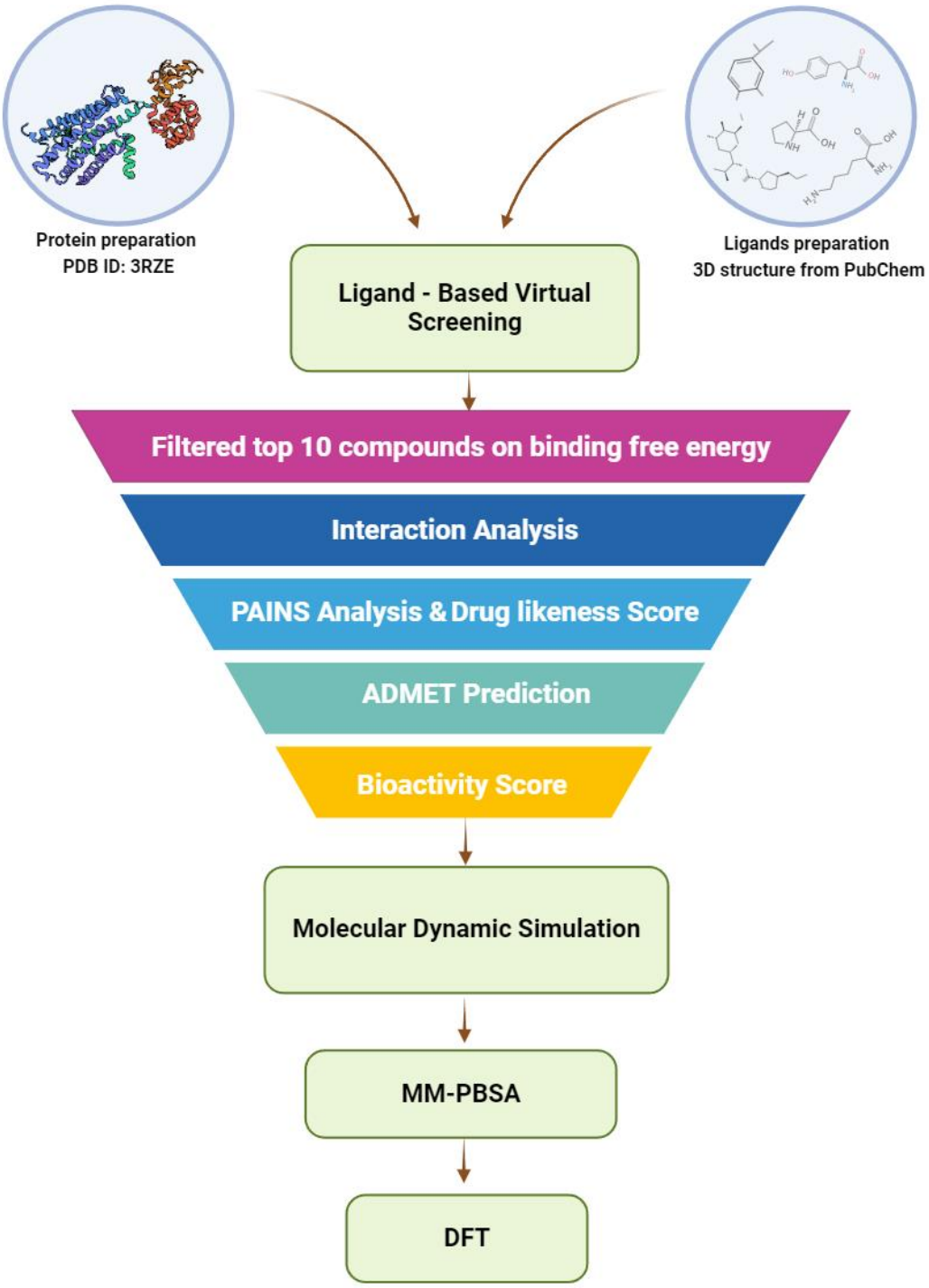

CHAPTER 1 INTRODUCTION

Allergy is a pervasive chronic condition with a global reach, affecting individuals across the world due to its lack of geographical boundaries. The escalating degradation of the environment, characterized by escalating levels of air and water pollution, stands as a foremost catalyst for allergic reactions. A multitude of allergy types exist, some of which are exceptionally severe, presenting life-threatening risks. Common contemporary allergy categories encompass pollen allergies, food allergies, insect sting allergies, and drug allergies(Zulfiqar et al., 2021) Food allergy is becoming more acknowledged as a significant public health issue and has been described as the "second wave" of the allergy epidemic, following asthma. A food allergy is a specific immune response to proteins found in food. This immune response can be either mediated by immunoglobulin (Ig)E or not mediated by IgE. The IgE-mediated food allergy is a global health issue that impacts a large number of individuals and various aspects of their lives. Food-induced allergic reactions can cause a range of symptoms affecting the skin, gastrointestinal tract, and respiratory tract. The exact prevalence rates are uncertain, but there is evidence to suggest that the incidence of this phenomenon has risen over the last thirty years, particularly in countries that have adopted a Western lifestyle. While it is possible for any type of food to trigger an allergic reaction, the majority of allergies are caused by only a small number of specific foods. The items in question are milk, eggs, peanuts, shellfish, wheat, and nuts. Recently, there have been numerous reports of life-threatening reactions occurring shortly after consuming food. Approximately 6% of children encounter food allergic reactions during the initial three years of their lives. This includes around 2.5% who have an allergy to cow's milk, 1.5% who have an allergy to eggs, and 1% who have an allergy to peanuts. Research has indicated that the prevalence of peanut allergies has risen in the last ten years (Pajno et al., 2018). Oral immunotherapy (OIT) induces immunomodulatory effects that result in desensitisation, which is characterised by decreased reactivity during active OIT, in the majority of treated individuals.

However, a smaller subset of treated subjects achieves sustained unresponsiveness after therapy discontinuation. The potential therapeutic benefits of OIT must be carefully considered in light of the significant risk of adverse events, which range from self-limited or easily treated oropharyngeal, respiratory, or gastrointestinal symptoms to persistent abdominal complaints that cause 10-15% of treated individuals to stop therapy.

1.1. Pathophysiology of Allergic Reaction

In the initial phase of an allergic response, a Type I hypersensitivity reaction is initiated. This involves the binding of allergens to antigen-presenting cells (APCs), leading to the activation of T-cells and subsequent secretion of interleukin-4 (IL-4). Activated T-cells then engage with B-cells, which are responsible for generating antibodies. During the interaction between B-cells and T-cells, IL-4 provides the necessary signal for B-cell activation, leading to the production of IgE antibodies. These IgE antibodies become affixed to mast cells through the FCεRI receptor. Upon subsequent exposure to the same allergen, the binding of allergens to IgE molecules causes cross-linking of IgE and FCεRI receptors. When more than one IgE receptor is engaged by the same allergen, mast cells are activated. (Banjare et al., 2020). The activated mast cells undergo degranulation, resulting in the release of bioactive compounds such as histamine, leukotrienes, prostaglandins, and other chemical mediators, which are the instigators of allergic reactions as shown in **Figure1**.

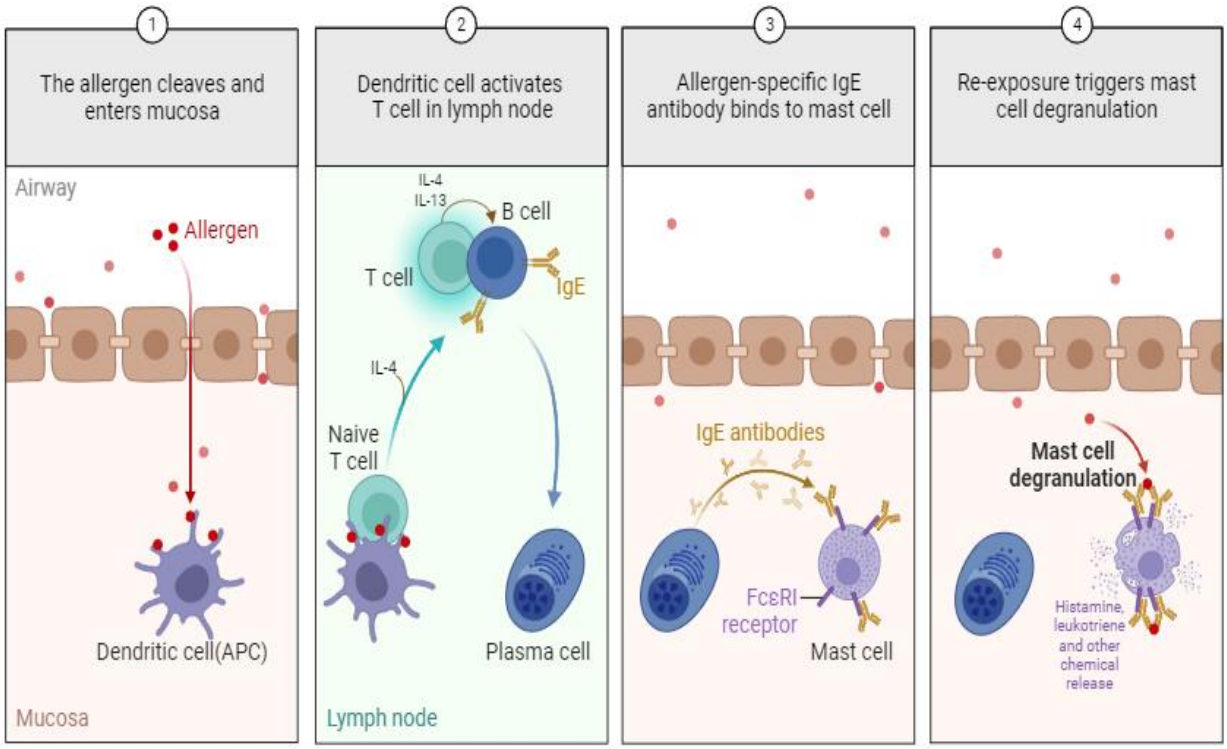

Figure 1: Pathophysiology of allergy reaction

Histamine is a nitrogenous organic compound involved in immune responses and an important neuro-transmitter which is chemically β- imidazolyethylamine. Histamine exerts its effects by binding to the receptor namely histamine receptor. There are four types of histamine receptor identified i.e., H_1R, H_2R, H_3R and H_4R. These receptors belong to G-

protein coupled receptors (GPCRs). Among the four histamine receptors, only H_1 and H_4 histamine receptors have a significant impact on allergic reactions. The histamine H_1 receptor plays a vital role in physiological processes, including inflammation, gastric acid secretion, mast cell-mediated chemotaxis, and neurotransmitter release when it binds to histamine. Histamine H_1 receptor belongs to the class I rhodopsin family of G protein-coupled receptors and triggers the activation of phospholipase C through interaction with G proteins. The protein (PDB ID – 3RZE) structure of the human Histamine H_1 receptor in complex with doxepin was selected. Antihistamine medications function by obstructing histamine's activity, preventing it from binding to its receptor.

In the past, first-generation antihistamine drugs such as clemastine, chlorpheniramine, and triprolidine were developed but exhibited substantial sedative properties and adverse effects on the central nervous system (CNS) and cholinergic system. These effects led to cognitive function impairment and low patient adherence to therapy. Second-generation antihistamine drugs like astemizole, cetirizine, and terfenadine were subsequently introduced to mitigate these side effects and reduce sedation. The model of second- generation H_1R antagonists will be highly beneficial for guiding rational design of ligands that do not penetrate the blood-brain barrier while maintaining H_1 selectivity(Shimamura et al., 2011). Consequently, cetirizine is best described as an inverse agonist in preference to a histamine antagonist, marketed as a racemic mixture containing both levocetirizine and dextrocetirizine(Chen et al., 2008). However, in later years, terfenadine and astemizole were withdrawn from the market due to their association with severe cardiovascular events(Estelle et al., 2020).

To enhance the biocompatibility and biodegradability of drug candidates, and to maximize efficacy, minimize risk, this research now engaged in the process of virtual screening, molecular docking, and simulations using novel natural anti-allergic compounds. These compounds are being investigated for their potential to target the Histamine H_1 receptor for anti-allergic therapeutic purposes.

CHAPTER 2 OBJECTIVES

1. Identification and preparation of a dataset of natural compounds with anti-allergic bioactivity

2. To virtually screen the anti- allergic compounds targeting Human Histamine H_1 Receptor

3. To determine the physio-chemical properties of the selected compounds

4. To check and validate the free energy, stability and binding affinity of the complex using MD simulation and MMPBSA studies

5. To examine and investigate the interaction and electronic structure using DFT method

CHAPTER 3 REVIEW OF LITERATURE

Allergy typically refers to the tissue damage or malfunctioning response that occurs when the immune system is exposed again to the same allergen(Hu et al., 2021). In the past few years, there has been an increase in the occurrence of allergic diseases, including food allergies, atopic dermatitis, allergic rhinitis, and asthma. Around 20-30% of the world's population is impacted and influenced by this phenomenon(Sabban, 2021). Researchers have focused on the development of advanced and beneficial medicinal compounds from both chemical and biological resources to effectively treat various types of allergies, in response to the growing demand for such treatments. The increasing demand and utilisation of these anti-allergy compounds have elevated the prominence of anti-allergy medications in the commercial pharmaceutical market.

The anti-allergy drugs market is expected to experience significant growth in the forecast period from 2021 to 2029, driven by the increased demand and usage seen in recent years. Based on market research analyses, the antihistamine drugs market had a value of USD 234.59 million in 2021 and is projected to reach USD 476.08 million by 2029(Andorf et al., 2017).Additionally, the global market value of topical corticosteroids is currently USD 4.85 billion in 2021 and is expected to increase to USD 8.08 billion by 2029(Andorf et al., 2017). Histamine plays a crucial role in causing localized hypersensitivity reactions. From a medical perspective, allergic reactions encompass a diverse array of effector cells and mediators. Based on the pathological mechanism, there are typically two types of allergic reactions: IgE-mediated and non-IgE-mediated allergic reactions. Allergies can result in a range of clinical symptoms such as nausea, vomiting, diarrhea, peptic ulcer, asthma, allergic dermatitis, allergic rhinitis, and other complications(Pajno et al., 2018). These complications can cause discomfort to the cardiovascular system, skin, respiratory tract, and digestive tract. Antihistamines exert their effects by attaching to one of the four identified histamine receptors. These receptors are present in hepatocytes, nerve cells, airway and vascular smooth muscles, and immune cells such as monocytes, neutrophils, and eosinophils.

G protein-coupled receptors (GPCRs) initiate physiological processes by detecting and attaching to a diverse array of extracellular stimuli, such as hormones, neurotransmitters, and various other small molecules. More than one third of drugs approved by the FDA are designed to target human GPCRs. GPCRs continue to be the primary focus for drug development in both academic and industrial laboratories. Histamine receptors belong to the

class A GPCRs and have been among the first GPCR targets in the rational drug development for treating diseases. Four histamine receptor subtypes in humans control essential physiological functions such as gastric acid secretion, smooth muscle relaxation, neurotransmitter release, and neutrophil distribution. The H_1 receptor (H_1R) subtype is present in various tissue types, such as the brain, vascular smooth muscle, airway, liver, and lymphocytes. Activation of the H_1 receptor (H_1R) triggers various physiological processes, such as the regulation of circadian rhythms, the body's reactions to allergens, and the production of pro-inflammatory cytokines. H_1 activation has also been linked to tumorigenesis associated with inflammation. Endogenous histamine's activation of H_1R is inhibited by commonly used medications called antihistamines, which are employed to prevent or diminish allergic reactions(O'Mahony et al., 2011). Due to the significant interest in discovering new H_1R drugs, more than 40 H_1R antagonists have been developed and approved for therapeutic use. The crystal structure of a human GPCR complexed with the antagonist doxepin, a first-generation antihistamine drug, was one of the first reported instances of such structures. Cetirizine is a diol mixture of R-levocetirizine and S-dextrocetirizine which belongs to the piperazine family. It relates to the group of early second-generation H_1 antihistamines (SGAHs) created to specifically inhibit the H1 receptor while minimizing binding to the central nervous system (CNS). It possesses advantageous pharmacological characteristics as it does not undergo interconversion, ensuring stability in the body. Additionally, it exhibits strong binding to serum albumin and has the lowest apparent volume of distribution. In addition, cetirizine demonstrates minimal penetration into the brain, low binding to lean tissues like the myocardium (resulting in minimal risk of heart toxicity), and minimal sedative effects. Cetirizine has demonstrated significant and swift absorption from the gastrointestinal tract, resulting in a high level of bioavailability and a rapid onset of drug efficacy(Wood et al., 1987). Cetirizine, unlike most other SGAHs, does not undergo significant hepatic metabolism. Instead, it is primarily excreted unchanged in the urine. This elimination process occurs equally well in both healthy individuals and patients with chronic liver disease. There is no need to adjust the dosage in the presence of abnormal liver function, but it is necessary to adjust the dosage in the case of renal dysfunction. The absence of hepatic metabolism indicates a minimal likelihood of drug-drug interactions, thereby preventing any excessive pharmacological or toxicological effects with drugs that undergo metabolism by P450 enzymes and transmembrane transport. The wheal and flare inhibition begins after 1 hour and lasts for 24 hours (Simons et al., 2004). Regarding safety, cetirizine has a minimal to nonexistent risk of causing harm to the heart.

Cetirizine has not been reported to have any harmful effects during pregnancy or while breastfeeding. Cetirizine has been classified by the Food and Drug Administration (FDA) as a pregnancy category B drug, meaning that it has not been found to cause harm to animal foetuses and there are no available human studies on its effects during pregnancy. While subjective assessments of the central nervous system (CNS) effects of cetirizine have yielded inconsistent results, studies that have used objective assessments such as driving and psychomotor performance tests have consistently shown that therapeutic doses of cetirizine do not typically cause more psychomotor impairment than a placebo. Moreover, studies have demonstrated that the side effects of cetirizine are similar to those of astemizole, ebastine, fexofenadine, loratadine, mizolastine, or terfenadine. These adverse effects of cetirizine are typically of mild-to-moderate severity. The ETAC study, which was the longest clinical trial of any antihistamine in the 20th century, involved children aged 18-24 months. The study found that continuous treatment with cetirizine for 18 months did not have any negative effects on neurological and behavioural events, or the normal development milestones of the children. This includes factors such as height, body mass, gross and fine motor skills, speech and language skills, as well as haematology and biochemistry tests. The incidence of treatment-emergent adverse events in the ETAC study, as reported by the investigators, was comparable between the cetirizine and placebo groups.
Levocetirizine is the biologically active form of cetirizine. Levocetirizine exhibits limited metabolism due to the absence of the CYP2D6 enzyme(Baltes et al., 2001). Dose adjustment is necessary only in cases of severe renal failure. The time required to reach the maximum concentration of a substance in the blood is 0.9 hours, and the time it takes for half of the substance to be eliminated from the body is 7.9 hours. The symptoms of allergic rhinitis showed improvement within 2 hours after administration of the medication(Horak et al., 2010). According to wheal and flare suppression tests, the time it takes for the medication to start working is 2 hours, and the duration of its effects is 24 hours. Levocetirizine is classified as FDA Pregnancy Category B, indicating that while there are no negative findings from animal studies, there is either no available data from human studies or there are positive findings from animal studies but no corresponding negative findings from human studies. The long-term safety of the second-generation H_1 antihistamines, desloratadine and loratadine, has been established through randomized controlled trials that lasted 6-18 months(Baltes et al., 2001). These trials included both adults and children as young as 1-2 years old. Loratadine is a piperidine-based oral medication that belongs to the second generation of histamine H1 receptor antagonists. It is metabolized by the liver's cytochrome

P450 system into its active form, known as desloratadine. Desloratadine is metabolized into 3-hydroxy desloratadine, which is then further metabolized through glucuronidation in the liver. It is shown that it is effective in treating seasonal allergic rhinitis (SAR) by reducing symptoms more than a placebo. The time it takes for the medication to start working has been extensively documented, ranging from 75 to 180 minutes in clinical settings(Tenn et al., 2018). The effects of the medication last for 24 hours. Dose adjustment is necessary only in the event of severe renal failure. There are very few negative effects reported when taking 10 mg of loratadine. Higher doses of the medication may result in central nervous system (CNS) effects that are directly proportional to the dosage. There is no evidence to suggest that overdosing on loratadine by up to 30 times the recommended dose has led to any serious negative effects or death(Wu et al., 2012). The effectiveness of treating persistent allergic rhinitis (PAR) in children aged 2-12 years was compared using loratadine syrup and cyproheptadine solution. The study done by Wu et al., 2012 , found that the loratadine group experienced a significant decrease in their total symptom score and an improvement in side effects related to the central nervous system. The study shows favorable long-term safety profiles in the 12-30 months age group during Phase I trials, with no significant adverse effects observed. The administering medication for 12 months, followed by a 12-month follow-up period in Phase II. Loratadine is classified as FDA Pregnancy Category B. Loratadine may be associated with a higher occurrence of hypospadias during pregnancy(Antonijoan et al., 2017). Desloratadine is a byproduct of loratadine (and rupatadine) and is efficiently broken down by the hepatic cytochrome P450 system. The specific enzymatic pathway responsible for the liver metabolism of desloratadine into 3-hydroxy desloratadine has not been documented as of yet. Desloratadine experiences lower first-pass metabolism compared to loratadine, which may result in reduced variability in the amount of desloratadine present in the body. Elimination takes place through both the renal and faecal pathways. Desloratadine has a minimal impact on its bioavailability when it interacts with drugs that affect transporter molecules. Among the second-generation antihistamines, desloratadine has the highest affinity for the H_1 receptor. Desloratadine demonstrated greater potency than fexofenadine and cetirizine in an in vitro study examining inverse agonism. This finding can be attributed to the strong correlation between H_1 receptor affinity and inverse agonist activity(Antonijoan et al., 2017). Desloratadine reaches its highest levels in the blood plasma at recommended doses for its antihistaminic effects, which are 10 times lower than the concentrations needed to observe its antimuscarinic effects in laboratory tests. At therapeutic doses, Desloratadine does not cause

any significant antimuscarinic effects that are relevant to clinical outcomes. There have been no reported instances of desloratadine interacting with cardiac potassium channels. Moreover, desloratadine does not negatively affect cognitive or psychomotor abilities, nor does it enhance the harmful effects of alcohol on psychomotor abilities(Potter et al., 2016). Even at doses up to 9 times the standard amount, no sedative effects have been reported. However, dose adjustment is necessary only in cases of severe renal failure. The wheal and flare response shows an onset of action after 2 hours, and the duration of action lasts for more than 24 hours. Desloratadine is classified as FDA Pregnancy Category C, indicating that there are no available or positive animal studies and no available human data regarding its effects during pregnancy. Desloratadine is authorised for the treatment of seasonal allergic rhinitis (SAR) in adults and children who are at least 2 years old, as well as for perennial allergic rhinitis (PAR) and chronic idiopathic urticaria in adults and children who are at least 6 months old, according to the prescribing information in the United States.
When taken orally, Rupatadine undergoes extensive metabolism. The drug's overall effectiveness may be attributed to the antihistaminic properties of two of its primary metabolites, desloratadine and 3-hydroxylated desloratadine. Despite its high degree of binding to human plasma proteins (98%–99%), rupatadine is effectively distributed in various tissues. This indicates that the compound is not trapped in the circulating blood and can easily reach its target receptors. Rupatadine undergoes significant hepatic metabolism, with CYP3A4 being identified as the primary isoenzyme responsible for its biotransformation. Therefore, it is advisable to exercise caution when using rupatadine in conjunction with CYP3A4 inhibitors and completely avoid its use with medications such as ketoconazole, azithromycin, fluconazole, and diltiazem. Exercise caution when combining rupatadine with drugs that have a narrow therapeutic range, as our understanding of its impact on other medications is limited(Barbanoj et al., 2004). Rupatadine is a second-generation H1 antihistamine that is effective in providing relief for allergic rhinitis. It has a rapid onset of action and is generally well tolerated by patients. It is referred to as a dual blocker because it inhibits both the activity of histamine and other inflammatory mediators, such as platelet-activating factors. This medication is recommended for the treatment of allergic rhinitis and chronic idiopathic urticaria in patients who are 2 years of age or older(Wu et al., 2012). The prompt assimilation of rupatadine is directly related to the initiation of its antihistamine and PAF effects, as determined by the inhibition of wheal and flare, which takes place within 1-2 hours after administration. There is a lack of sufficient studies conducted on pregnant women, and the prescribing information advises against using this product in pregnant

women. Preclinical studies revealed that rats experienced foetal toxicity, including growth delay, incomplete ossification, and minor skeletal findings. However, this toxicity was observed only at materno-toxic dose levels of 25 and 120 mg/kg/day. No signs of developmental toxicity were observed in rabbits even when administered doses as high as 100 mg/kg(Antonijoan et al., 2017). Rupatadine exhibits analogous behaviour to second-generation antihistamines in the central nervous system (CNS). Rupatadine exhibits psychomotor impairment effects solely at the maximum dosage of 80 mg, which is four times higher than the recommended therapeutic dose. No anticholinergic effects were detected in various preclinical models at doses of up to 7 mg/kg (more than 40 times the expected human dose) or single doses ranging from 10 to 80 mg in humans. The multiple centres compared the effectiveness of an oral solution of rupatadine in children aged 2-11 years with persistent allergic rhinitis to a placebo. The rupatadine was affected in reducing both nasal and non-nasal symptoms, and also improved the quality of life of the children. Fexofenadine is a biologically active substance that is produced when terfenadine is metabolised. Fexofenadine is currently a commonly utilised substitute for terfenadine, which carries a potential for causing serious ventricular arrhythmia. It exhibits low metabolic activity by cytochrome P450 and is mainly found in the gastrointestinal tract. The transport of fexofenadine is facilitated by certain transporters, namely P-gp, organic anion transporting polypeptide (OATP) 2B1, and multidrug resistance-associated protein 2 (MRP2)(Akamine et al., 2019). Fexofenadine has been classified by the FDA as Pregnancy Category C. The decrease in the weight and survival of offspring, and there is no available human data on the effects of fexofenadine(Barbanoj et al., 2004)

Tool/Software Name	Link (website)	Reference
PubChem Database	https://pubchem.ncbi.nlm.nih.gov/	(Kim et al., 2023)
PyMol	https://pymol.org/2/	(Schrodinger et al., 2020)
Protein Data Bank	https://www.rcsb.org/structure/3RZE	(Berstein et al., 1977)
SWISS MODEL	https://swissmodel.expasy.org/	(Waterhouse et al., 2018)
AutoDock Vina	https://vina.scripps.edu/	(Trott et al., 2010)
BIOVIA Discovery Studio Visualizer	https://discover.3ds.com/discovery-studio-visualizer-download	(Biovia et al., 2000)
DrugLiTo	https://niper.gov.in/pi_dev_tools/DruLiToWeb/DruLiTo_index.html	(Kerns et al., 2008)
ADMETLab2.0	https://admetmesh.scbdd.com/	(Xiong et al., 2021)
Molinspiration Cheminoformatics	https://www.molinspiration.com/	(Hadda et al., 2021)
GROMACS	https://www.gromacs.org/	(Abraham et al., 2015)
Gaussian 09W	https://gaussian.com/glossary/g09/	(Frisch et al., 2016)
Gauss View 6.0 visualization	https://gaussian.com/gaussview6/	(Frisch et al., 2016)

CHAPTER 4 MATERIALS AND METHODS

4.1. Ligand identification and preparation:

The dataset of ligands was based on the novel compounds derived from algae, sponges, fungi, and plants, showing potential for anti-allergy properties. The 3D structure in SDF file format, SMILES, and 2D structure were retrieved from PubChem database along with their PubChem IDs. The ligands were converted into PDB file format using PyMol software. The AutoDock MGL tool was used to convert the PDB format to the PDBQT file format for further analysis.

4.2. Protein identification and preparation:

Histamine is a major linking bridge between allergic reactions and the H1 receptor. The human histamine receptor membrane protein in complex with Doxepin, (3RZE) PDB file was downloaded from the Research Collaboratory for Structural Bioinformatics Protein Data Bank. Due to the missing residues present in the 3RZE protein, pairwise sequence alignment was done with 7DFL FASTA as a template using EMBOSS Needle software. Then, the SWISS MODEL was used to model the protein. PyMol was used to remove the antagonist, Doxepin from the desired protein structure. The AutoDock MGL tool was used to prepare the structure by deleting water molecules, adding hydrogen atoms, and partial atomic charge for molecular docking. The resultant protein structure was then saved in PDBQT format for further analysis.

4.3. Molecular Docking:

The prepared structure of ligand and protein in PDBQT format was used to generate the potential grid box using the AutoDock MGL tool, for site-specific docking. The config file in text format was created with valid information on the receptor, ligand, center, size, energy range, and exhaustiveness to conduct molecular docking. The AutoDock Vina tool was used to generate binding affinity (kCal/mol) and distance from best mode i.e., root mean square deviation (rmsd) Upper bound and Lower bound within ligand and protein interactions. The lowest binding energies of ligands were considered for further analysis. The best docking pose of protein-ligand complexes generated were visualized by PyMol and saved in PDB format.

4.4. Interaction Analysis:

The various 2D and 3D visualizations and interaction of participating residual and atomic coordinates within docked protein-ligand complexes were explored by BIOVIA Discovery Studio Visualizer software. The different interaction patterns were identified like interacting amino acids, bond type (H-bonds, hydrophobic, and electrostatic) along with their respective bond lengths.

4.5. PAINS (Pan-assay interference compounds) filters and Drug likeness score:

To ensure that the selected compounds have pharmacokinetic properties, various molecular filters were used. The software DrugLiTo 1 (Drug Likeness Tool) is used as an open-source virtual screening tool to calculate different molecular properties of the ligands. The SDF file format of the compound was used to calculate the properties. The various parameters applied to evaluate the compounds are Lipinski's rule (no. of HBD<5, no. of HBA <10, molecular weight <500 and ClogP<5), MDDR (no. of rings >3, no. of rigid bonds >18 and no. of rotatable bonds >6), Ghose rule (logP, molar refractivity, molecular weight, no. of atoms and polar surface area < 140). The compound that passes all of Lipinski's rules was ethically considered. Molsoft software tool is used to predict the drug-likeness score and model the graph of selected ligands.

4.6. ADMET Analysis:

The canonical SMILES of the considered ligands were used as input in the web server ADMETlab2.0. This server provides pharmacokinetic properties like absorption (caco-2 permeability, Pgp-inhibitor, MDCK permeability and HIA), distribution (PPB, VD, BBB Penetration and Fu), metabolism (CYP1A2, CYP2C19, CYP2C9, CYP2D6 and CYP3A4), excretion (CL and T½) and toxicity (hERG blockers, DILI, AMES toxicity, H-HT, Rat oral acute toxicity, FDAMDD, skin sensitization, eye corrosion and irritation, respiratory, acute toxicity rule, carcinogenicity, genotoxic carcinogenicity rule and non-genotoxic carcinogenicity rule).

4.7. Bioactivity Score:

The potential of the selected compounds to be a drug candidate can be evaluated by drug score value. The web-based tool, Molinspiration cheminformatics was used to predict the bioactivity score of the compounds against the regular human receptor such as kinase

inhibitor, nuclear receptor ligand, GPCR ligand, ion channel modulator proteases inhibitor and enzymes inhibitor.

4.8. Molecular dynamic simulation (MDS):

The protein-ligand structure which was generated from molecular docking was assessed using Molecular Dynamic (MD) simulation. This method predicts the behavior and conformational changes of a protein at atomic level and accurate temporal resolution. The software program GROMACS version 2020.1 as used to enhance the structure. The ligand topology was generated using PRODRG, while the protein topology was created using pdb2gmx. An additional approach applied to equilibrate the systems was NPT and NVT simulation. Protein and protein-ligand complex trajectories were examined using the following methods: solvent-accessible surface area analysis (SASA), hydrogen bond analysis, along with hydrogen distribution, compactness analysis via a radius of gyration (Rg), principal component (PC) analysis, flexibility analysis via root-mean-square-fluctuation (RMSF) and structural stability analysis via root-mean-square-deviation (RMSD). The calculations for potential energy, kinetic energy, total energy, conserved energy, temperature, and pressure were also performed. The data were analysed and visualised with the 2D plotting program Grace.

4.9. Molecular mechanics Poisson-Boltzmann surface area (MMPBSA):

High-throughput molecular dynamics simulations were employed to conduct binding free energy calculations for selected protein-ligand complexes utilizing the g_mmpbsa tool. The free energy linked with the binding of the protein-ligand complex denoted as $G_{binding}$, is expressed as the difference between the total binding free energy of the complex ($G_{complex}$) and the sum of the free energies of the unbound receptor ($G_{protein}$) and the unbound ligand (G_{ligand}).

$$\Delta G_{binding} = G_{complex} - (G_{protein} + G_{ligand})$$

4.10. Density functional theory (DFT):

The computational quantum mechanical modelling or DFT is a method use to conduct the electronic structure along with the investigation of protein-ligand interaction(Sabe et al., 2021). The initial geometry of lead molecules was optimized using the Gaussian 09W

software package, employing the DFT/B3LYP method and the 6-311G, ++, (d,p) parameter set. The optimized molecular structure, frequency, FMOs, molecular electrostatic potential surface, and Mulliken charges were visualized using the Gauss View 6.0 visualization tool. An analysis of charge transfer within the compounds was conducted using a HOMO-LUMO study. The chemical potential and hardness were derived from the lowest unoccupied molecular orbital (LUMO) and highest occupied molecular orbital (HOMO) values. A natural population analysis was conducted to examine the inherent energies of a single atom within the lead molecules.

5.1. Formation of Dataset:

Virtual screening is a technique used to find an optimal screening between large molecules (macromolecular targets) and small molecules (like drugs) by searching through literature and databases of chemical compounds. This method predicts the ligands that will interact most efficiently with an antagonist to form a stable complex. **Table 1** are the list of natural compounds along with their Pubchem IDs, source of isolation, SMILES and 2D structure.

Table 1: Dataset of natural compounds having Anti-Allergic activity

COMPOUND NAME (Pubchem Ids)	SOURCE OF ISOLATION	SMILES	2-D STRUCTURE
Fucodiphloroethol G (44590821)	*Ecklonia cava*	C1=C(C=C(C(=C1O)C2=C(C=C(C=C2OC3=C(C=C(C=C3OC4=C(C=C(C=C4O)O)O)O)O)O)O)O)O	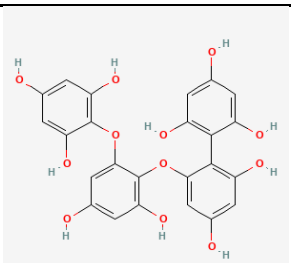
Eckol (145937)	*Ecklonia cava*	C1=C(C=C(C=C1O)OC2=C(C=C(C3=C2OC4=C(C=C(C=C4O3)O)O)O)O)O	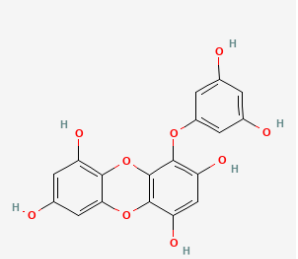
Phlorofucofuroeckol A (130976)	*Ecklonia cava*	C1=C(C=C(C=C1O)OC2=C(C=C(C3=C2OC4=C3C5=C(C(=C4)O)OC6=C(O5)C(=CC(=C6OC7=CC(=CC(=C7)O)O)O)O)O)O)O	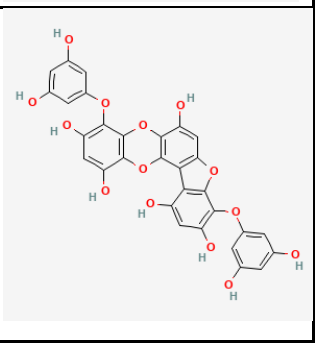

Fucofuroeckol-A (2342671)	*Ecklonia stolonifera Okamura*	CC(=O)OC1=CC(=CC(=C1)OC2=C(C=C(C3=C2OC4=C(C=C5C(=C4O3)C6=C(O5)C=C(C=C6OC(=O)C)OC(=O)C)OC(=O)C)OC(=O)C)OC(=O)C)OC(=O)C)OC(=O)C	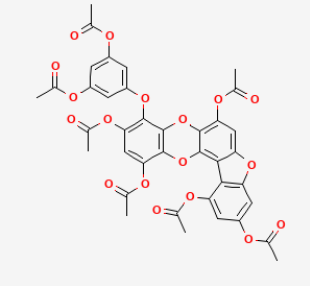
6,6’-Bieckol (137388)	*Eisenia arborea*	C1=C(C=C(C=C1O)OC2=C(C=C(C3=C2OC4=C(C=C(C(=C4O3)C5=C6C(=C(C=C5O)O)OC7=C(O6)C(=CC(=C7OC8=CC(=CC(=C8)O)OO)O)O)O)O)O)O	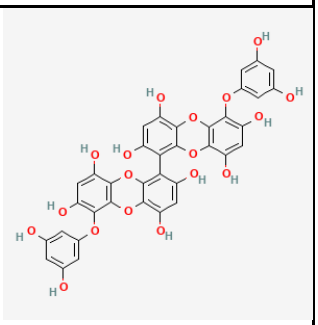
6,80-Bieckol (57523992)	*Eisenia arborea*	C1=C(C=C(C=C1O)OC2=C(C=C(C3=C2OC4=C(O3)C=C(C(=C4O)C5=C6C(=C(C=C5O)O)OC7=C(O6)C(=CC(=C7OC8=CC(=CC(=C8)O)O)O)O)O)O)O)O	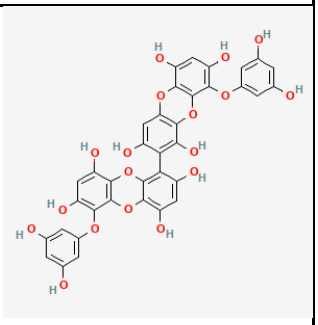
8,80-Bieckol (3008867)	*Eisenia arborea*	C1=C(C=C(C=C1O)OC2=C(C=C(C3=C2OC4=C(O3)C=C(C(=C4O)C5=C(C6=C(C=C5O)OC7=C(O6)C(=C(C=C7O)O)OC8=CC(=CC(=C8)O)O)O)O)O)O)O	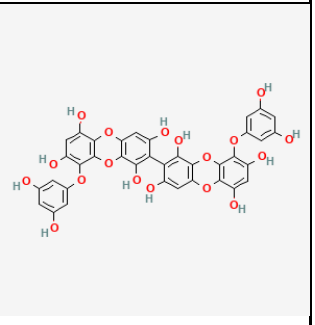

Phlorofucofuroeckol-B (15984097)	*Eisenia arborea*	C1=C(C=C(C=C1O)O C2=C(C=C(C3=C2OC 4=CC5=C(C(=C43)O) OC6=C(O5)C(=CC(=C 6OC7=CC(=CC(=C7) O)O)O)O)O)O)O	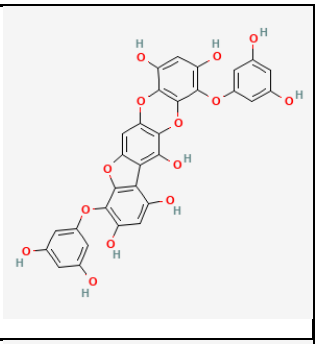
Izp-94005 (164397)	*Petrosia sp.*	CC(C)C1CC(OC(C1)O)C(C)C2CC(=O)C3C2(CCC4C3C(C(C5C4(C CC(C5O)O)C)O)O)C	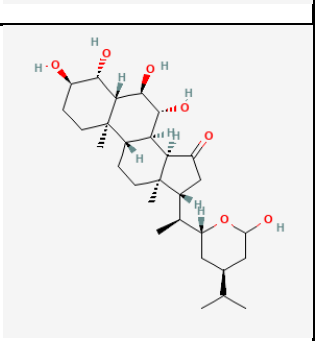
Penasterone (10321758)	*Penares incrustans*	CC(CCC=C(C)C)C1C CC2(C1(CCC3=C2CC C4C3(CCC(=O)C4(C) C)C)C)C(=O)O	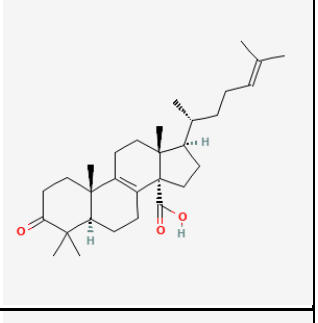
Xestobergsterol A (124015)	*Xestospongia bergquistia, Penares incrustans*	C1CC(C2C1C3(CCC4 C(C3C2=O)C(C(C5C4 (CCC(C5)O)C)O)O)C) (CC(C)C)O	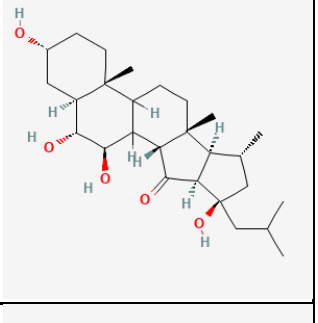
Xestobergsterol B (15167969)	*Xestospongia bergquistia, Penares incrustans*	CC1CC(C2C1C3(CCC 4C(C3C2=O)C(C(C5C 4(C(C(C(C5)O)O)O)C) O)O)C)(CC(C)C)O	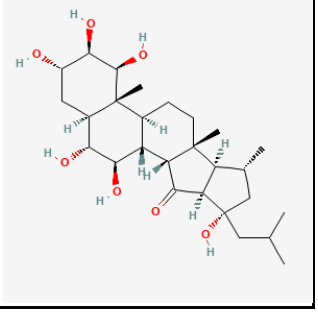

Penasterol (164003)	*Xestospongia bergquistia, Penares incrustans*	CC(CCC=C(C)C)C1CCC2(C1(CCC3=C2CCC4C3(CCC(C4(C)C)O)C)C)C(=O)O	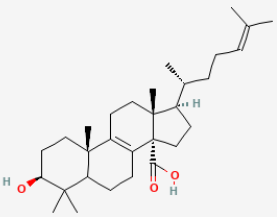
Reticulol (5359036)	*Graphostroma sp. Botryotinia fuckeliana*	CC1=CC2=CC(=C(C(=C2C(=O)O1)O)OC)O	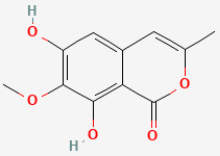
Botryotin A (156582914)	*Graphostroma sp. Botryotinia fuckeliana*	CC(=O)OCC1(CCC2C1CC3=C2C4(CCC(C(C4CC3)(C)CO)O)C)O	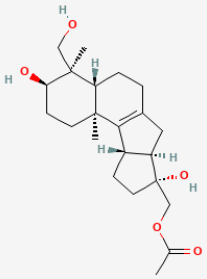
Viridicatol (115033)	*Penicillium*	C1=CC=C2C(=C1)C(=C(C(=O)N2)O)C3=CC(=CC=C3)O	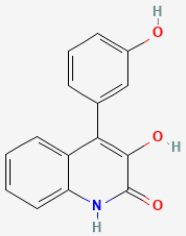
Ethyl-(E)–Undec-6-Enoate (14570631)	*M. oleifera extracts (drumstick tree)*	CCCCC=CCCCCC(=O)OCC	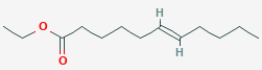

3,5,6-Trihydroxy-2-(2,3,4,5,6-Pentahydroxyphenyl)-4H-Chromen-4-One (145706543)	*M. oleifera extracts*	C1=CC2=C(C(=C1O)O)C(=O)C(=C(O2)C3=C(C(=C(C(=C3O)O)O)O)O)O	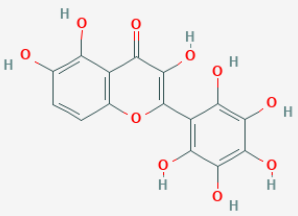
Quercetin (5280343)	*M. oleifera extracts*	C1=CC(=C(C=C1C2=C(C(=O)C3=C(C=C(C=C3O2)O)O)O)O)O	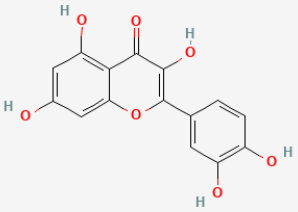
Kaempferol (5280863)	*M. oleifera extracts*	C1=CC(=CC=C1C2=C(C(=O)C3=C(C=C(C=C3O2)O)O)O)O	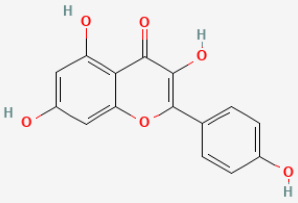
Oleic Acid (445639)	*M. oleifera extracts*	CCCCCCCCC=CCCCCCCCC(=O)O	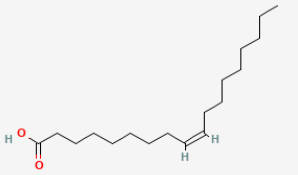
Glucomoringin (162639104)	*M. oleifera extracts*	CC1C(C(C(C(O1)OC2=CC=C(C=C2)CC(=NOS(=O)(=O)[O-])SC3C(C(C(C(O3)CO)O)O)O)O)O)O.[K+]	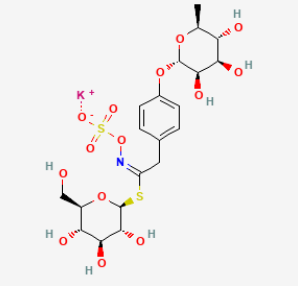

2,3,4-Trihydroxybenzaldehyde (75064)	*M. oleifera extracts*	C1=CC(=C(C(=C1C=O)O)O)O	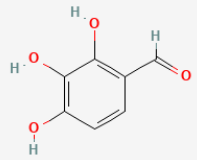
Stigmasterol (5280794)	*M. oleifera extracts*	CCC(C=CC(C)C1CCC2C1(CCC3C2CC=C4C3(CCC(C4)O)C)C)C(C)C	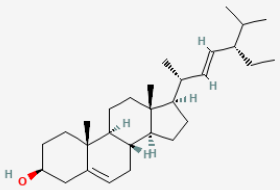
Epigallocatechin Gallate (65064)	*green tea*	C1C(C(OC2=CC(=CC(=C21)O)O)C3=CC(=C(C(=C3)O)O)O)OC(=O)C4=CC(=C(C(=C4)O)O)O	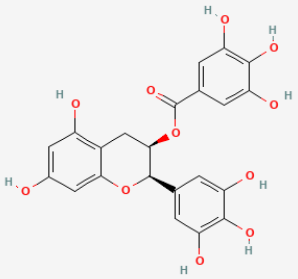
Curcumin (969516)	*Curcuma longa (turmeric)*	COC1=C(C=CC(=C1)C=CC(=O)CC(=O)C=CC2=CC(=C(C=C2)O)OC)O	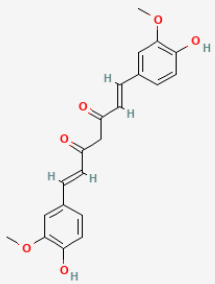
Gingerol (442793)	*Zingiber officinale (ginger)*	CCCCCC(CC(=O)CCC1=CC(=C(C=C1)O)OC)O	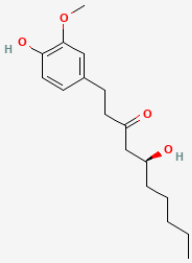

Rosmarinic Acid (5281792)	*Rosemary (Rosmarinus officinalis) and basil (Ocimum basilicum)*	C1=CC(=C(C=C1CC(C(=O)O)OC(=O)C=CC2=CC(=C(C=C2)O)O)O)O	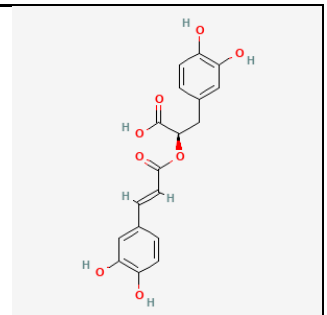
Myricitrin (5281673)	*Sonneratia caseolaris (L.) fruit extract (mangrove apple)*	CC1C(C(C(C(O1)OC2=C(OC3=CC(=CC(=C3C2=O)O)O)C4=CC(=C(C(=C4)O)O)O)O)O)O	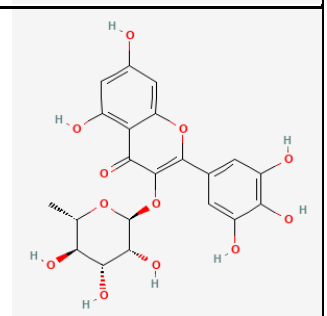
Luteolin (5280445)	*Perilla (Perilla frutescens) (beefsteak)*	C1=CC(=C(C=C1C2=CC(=O)C3=C(C=C(C=C3O2)O)O)O)O	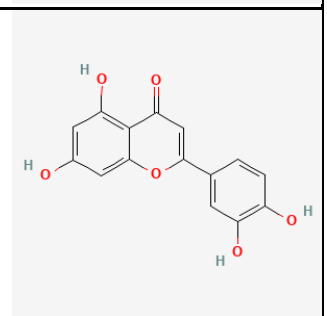
Triterpene (24825667)	*Luffa cylindrica (sponge gourd)*	C[C]12CCC(=O)C(C1CC[C]3([CH]2CC=C4[C]3(CC[C]5([CH]4CC(CC5)(C)C)C(=O)O)C)C)(C)C	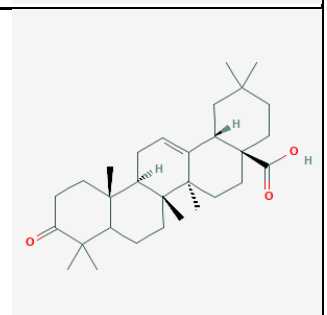
Bryonolic Acid (472768)	*Citrullus lanatus (water melon)*	CC1(C2CCC3=C(C2(CCC1O)C)CCC4(C3(CCC5(C4CC(CC5)(C)C(=O)O)C)C)C)C	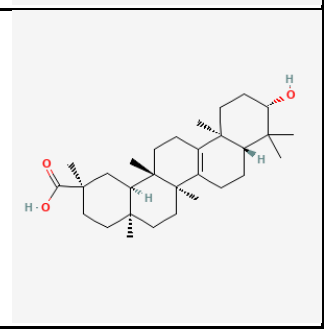

Astragaloside V (71448939)	*Astragalus membranaceus (locoweed)*	CC1(C(CCC23C1C(CC4C2(C3)CCC5(C4(CC(C5C6(CCC(O6)C(C)(C)OC7C(C(C(C(O7)CO)O)O)O)C)O)C)C)O)OC8C(C(C(CO8)O)O)OC9C(C(C(C(O9)CO)O)O)O)C	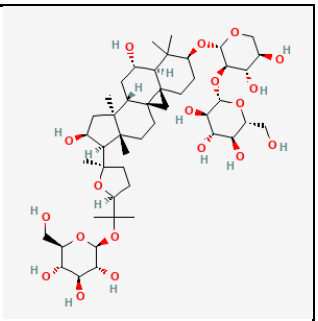
Asiminecin (10722577)	*Artemisia annua (sweet wormwood)*	CCCCCC(CCCCC(C1CCC(O1)C2CCC(O2)C(CCCCCCCCCCCC3=CC(OC3=O)C)O)O)O	
Usnic Acid (5646)	*lichen Roccella montagnei*	CC1=C(C(=C2C(=C1O)C3(C(=CC(=O)C(C3=O)C(=O)C)O2)C)C(=O)C)O	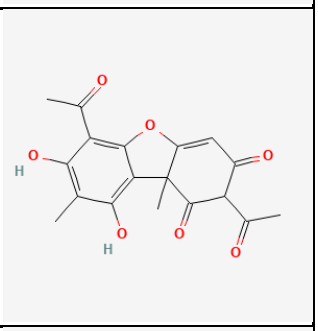
Gericudranins A (10436583)	*Cudrania tricuspidata*	C1=CC(=CC=C1CC2=C(C(=C3C(=C2O)C(=O)C(C(O3)C4=CC(=C(C=C4)O)O)O)CC5=CC=C(C=C5)O)O)O	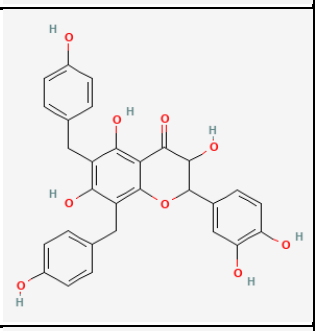
Astragaloside-II (71306915)	*Astragalus membranaceus (milkvetches)*	CC(=O)OC1C(C(COC1OC2CCC34CC35CCC6(C(C(CC6(C5CC(C4C2)OC7C(C(C(C(O7)CO)O)O)O)C)O)C8(CCC(O8)C(C)(C)O)C)C)O)O	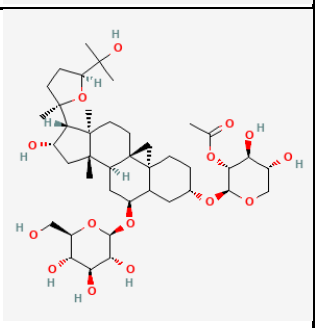

Coriaheptocin B (44566649)	*Annona coriacea Mart*	CCCCCCCCCCCCC(C(CCC(CC(CC(C1CCC(O1)C(CCC(CC2=CC(OC2=O)C)O)O)O)O)O)O)O)O	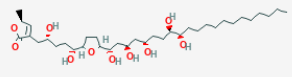
Paucin (161538)	*Baileya pauciradiata (laxflower)*	CC1CC2C(CC3(C1C(CC3=O)OC4C(C(C(C(O4)COC(=O)C)O)O)O)C)C(=C)C(=O)O2	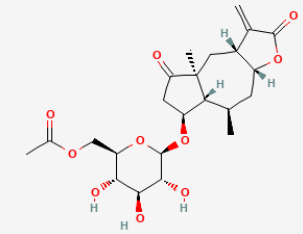
Chebulinic Acid (16745534)	*Terminalia chebula (black-myrobalan)*	C1=C(C=C(C(=C1O)O)O)C(=O)OCC2C3C(C(C(O2)OC(=O)C4=CC(=C(C(=C4)O)O)O)OC(=O)C5=CC(=C(C6=C5C(C(C(=O)O3)CC(=O)O)C(C(=O)O6)O)O)O)OC(=O)C7=CC(=C(C(=C7)O)O)O	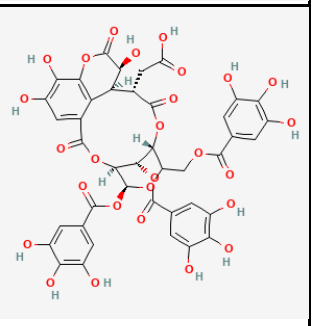
Astragalin (5282102)	*Cuscuta chinensis Lam.*	C1=CC(=CC=C1C2=C(C(=O)C3=C(C=C(C=C3O2)O)O)OC4C(C(C(C(O4)CO)O)O)O)O	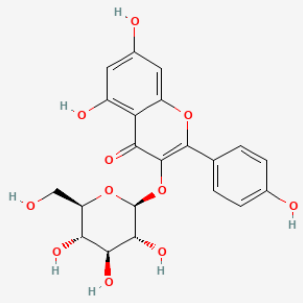
Karavilagenin E (66559251)	*Momordica balsamina (balsam apple)*	CC(CC(C=C(C)C)O)C1CCC2(C1(CCC34C2C=CC5(C3CCC(C5(C)C)O)OC4)C)C	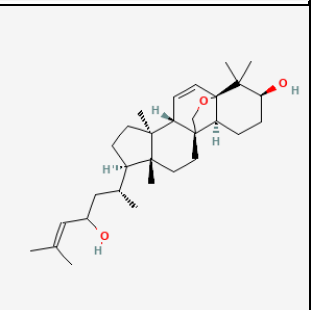

Kosamol A (10250640)	*Sophora flavescens*	CC(=CCC(CC1=C2C(=C(C(=C1O)CCC(C)(C)O)O)C(=O)C(C(O2)C3=C(C=C(C=C3)O)O)O)C(=C)C)C	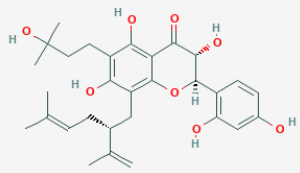
Kenusanone A (10365031)	*Eryngium caeruleum (sea holy)*	CC(=CCCC(=CCC1=CC(=C(C=C1O)O)C2COC3=CC(=CC(=C3C2=O)O)O)C)C	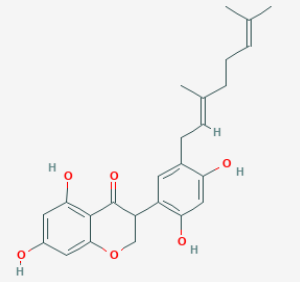
Kushenol C (5481237)	*Sophora flavescens aiton*	CC(=CCC(CC1=C2C(=C(C=C1O)O)C(=O)C(=C(O2)C3=C(C=C(C=C3)O)O)O)C(=C)C)C	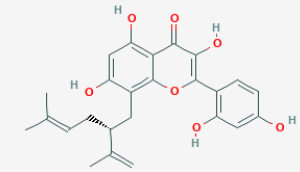
Zerumbone (5470187)	*Z. zerumbet (wild ginger)*	CC1=CCC(C=CC(=O)C(=CCC1)C)(C)C	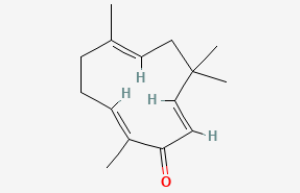
Humulene (5281520)	*Z. zerumbet*	CC1=CCC(C=CCC(=CCC1)C)(C)C	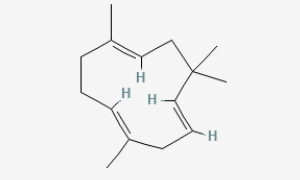

Linalool (6549)	*Z. zerumbet*	CC(=CCCC(C)(C=C)O)C	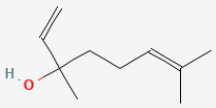
Caryophyllene (5281515)	*Z. zerumbet*	CC1=CCCC(=C)C2CC(C2CC1)(C)C	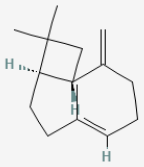
Limonene (22311)	*Z. zerumbet*	CC1=CCC(CC1)C(=C)C	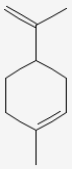
Desacetylmatricarin (6713966)	*Taraxacum platycarpum*	CC1C2C(CC(=C3C(C2OC1=O)C(=CC3=O)C)C)O	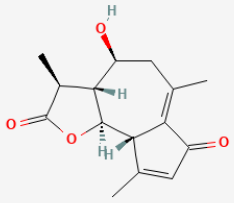
Bergenin (66065)	*Connarus semidecandrus*	COC1=C(C=C2C(=C1O)C3C(C(C(C(O3)CO)O)O)OC2=O)O	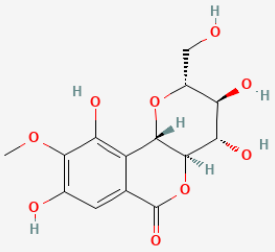

Barakol (3080731)	*Cassia siamea (johar)*	CC1=CC2=C3C(=CC(=C2)O)OC(=CC3(O1)O)C	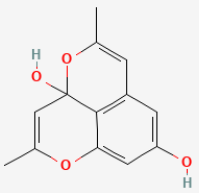
Strictosidinic Acid (21586927)	*Hunteria zeylanica*	C=CC1C(C(=COC1OC2C(C(C(C(O2)CO)O)O)O)C(=O)O)CC3C4=C(CCN3)C5=CC=CC=C5N4	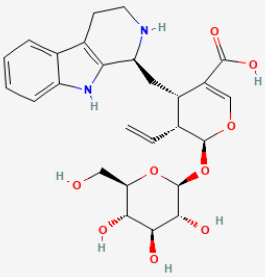
Lawsone Methyl Ether (16871)	*Impatiens balsamina (balsam)*	COC1=CC(=O)C2=CC=CC=C2C1=O	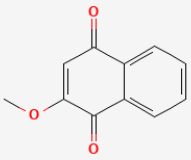
Tachioside (11962143)	*Lindera obtusiloba (Japanese spicebush)*	COC1=C(C=CC(=C1)OC2C(C(C(C(O2)CO)O)O)O)O	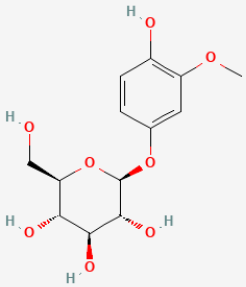
Isotachioside (15098566)	*Lindera obtusiloba*	COC1=C(C=CC(=C1)O)OC2C(C(C(C(O2)CO)O)O)O)O	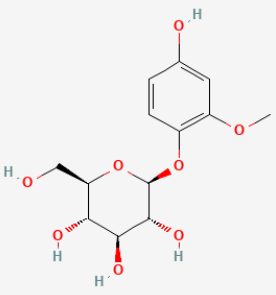

Koaburaside (5318820)	*Lindera obtusiloba*	COC1=CC(=CC(=C1O)OC)OC2C(C(C(C(O2)CO)O)O)O	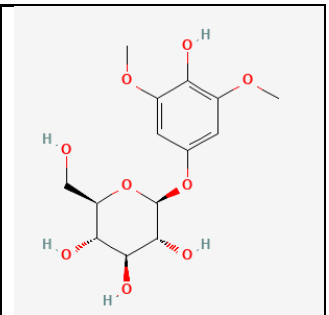
Salidroside (159278)	*Lindera obtusiloba*	C1=CC(=CC=C1CCOC2C(C(C(C(O2)CO)O)O)O)O	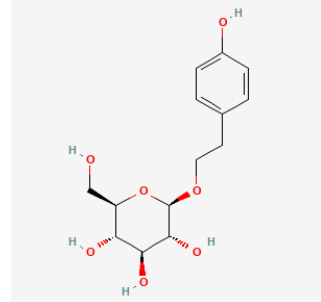
Baicalin (64982)	*Scutellaria baicalensis (Chinese skullcap)*	C1=CC=C(C=C1)C2=CC(=O)C3=C(C(=C(C=C3O2)OC4C(C(C(C(O4)C(=O)O)O)O)O)O)O	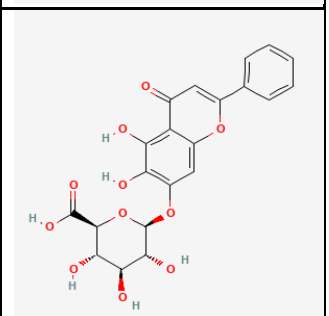
Isoquercitrin (5280804)	*Hops (Humulus lupulus L.); onion (Allium cepa)*	C1=CC(=C(C=C1C2=C(C(=O)C3=C(C=C(C=C3O2)O)O)OC4C(C(C(C(O4)CO)O)O)O)O)O	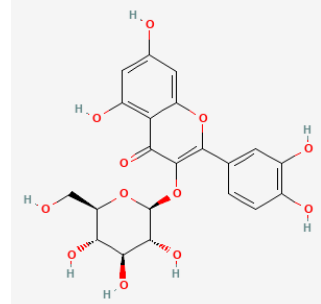
Fisetin (5281614)	*Rhus verniciflua Seeds.*	C1=CC(=C(C=C1C2=C(C(=O)C3=C(O2)C=C(C=C3)O)O)O)O	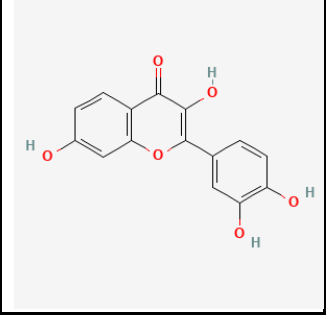

Myricitin (5281672)	*Abelmoschus moschatus (musk mallow)*	C1=C(C=C(C(=C1O)O)O)C2=C(C(=O)C3=C(C=C(C=C3O2)O)O)O	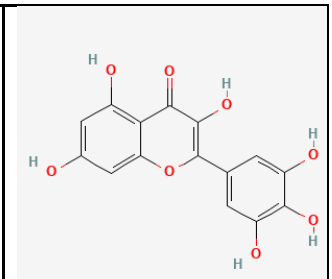
Rutin (5280805)	*E. pulcherrima (poinsettia)*	CC1C(C(C(C(O1)OCC2C(C(C(C(O2)OC3=C(OC4=CC(=CC(=C4C3=O)O)O)C5=CC(=C(C=C5)O)O)O)O)O)O)O)O	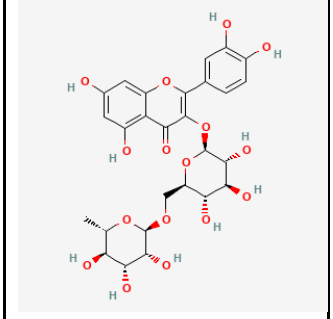
Galangin (5281616)	*Rhizoma Alpiniae Officinarum (lesser galangal)*	C1=CC=C(C=C1)C2=C(C(=O)C3=C(C=C(C=C3O2)O)O)O	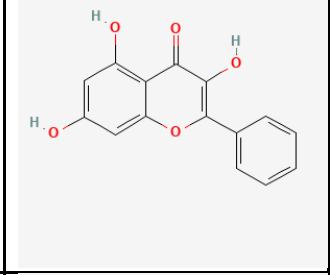
Silymarin (5213)	*Silybum marianum (milk thistle)*	COC1=C(C=CC(=C1)C2C(OC3=C(O2)C=C(C=C3)C4C(C(=O)C5=C(C=C(C=C5O4)O)O)O)CO)O	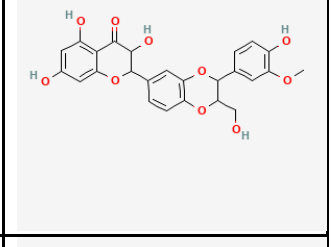
Gossypin (5281621)	*Hibiscus vitifolius (grape-leaved mallow)*	C1=CC(=C(C=C1C2=C(C(=O)C3=C(O2)C(=C(C=C3O)O)OC4C(C(C(C(O4)CO)O)O)O)O)O)O	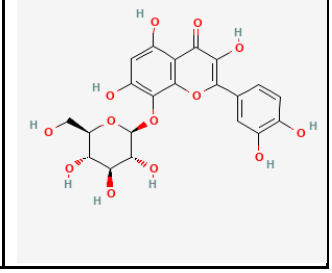

Ayanin (5280682)	*Psychotria serpens*	COC1=C(C=C(C=C1)C2=C(C(=O)C3=C(C=C(C=C3O2)OC)O)OC)O	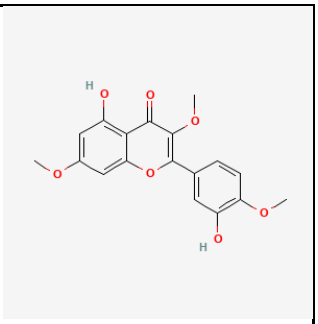
Epicatechin (72276)	*Dalbergia monetaria (moneybush)*	C1C(C(OC2=CC(=CC(=C21)O)O)C3=CC(=C(C=C3)O)O)O	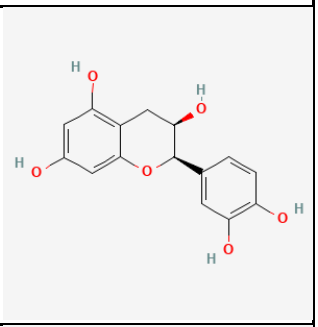
Eriodictyol (440735)	*Eriodictyon californicum (gum plant)*	C1C(OC2=CC(=CC(=C2C1=O)O)O)C3=CC(=C(C=C3)O)O	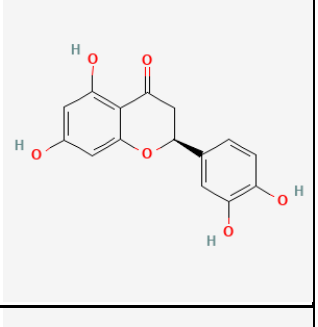
Daidzein (5281708)	*green peas (Pisum sativum) and black beans (Phaseolus vulgaris)*	C1=CC(=CC=C1C2=COC3=C(C2=O)C=CC(=C3)O)O	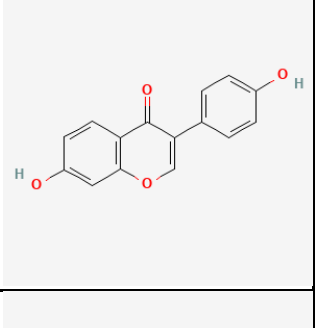
Genistein (5280961)	*green peas (Pisum sativum) and black beans (Phaseolus vulgaris)*	C1=CC(=CC=C1C2=COC3=CC(=CC(=C3C2=O)O)O)O	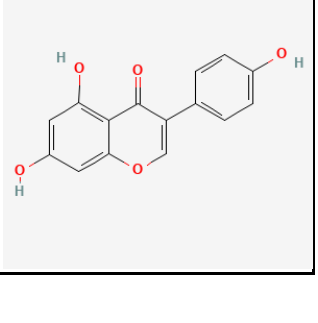

Glycitein (5317750)	*green peas (Pisum sativum) and black beans (Phaseolus vulgaris)*	COC1=C(C=C2C(=C1)C(=O)C(=CO2)C3=CC=C(C=C3)O)O	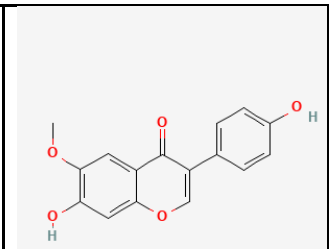
Puerarin (5281807)	*Pueraria lobata*	C1=CC(=CC=C1C2=COC3=C(C2=O)C=CC(=C3C4C(C(C(C(O4)CO)O)O)O)O)O	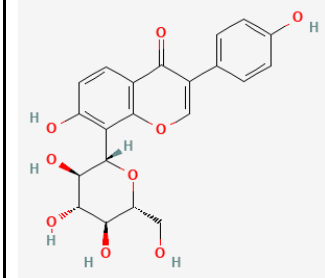
Apigenin (5280443)	*Symphyotrichum novae-angliae (aster)*	C1=CC(=CC=C1C2=CC(=O)C3=C(C=C(C=C3O2)O)O)O	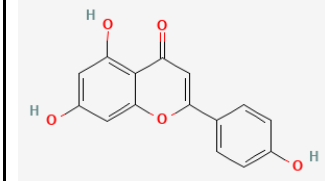
Diosmetin (5281612)	*S. montana L.*	COC1=C(C=C(C=C1)C2=CC(=O)C3=C(C=C(C=C3O2)O)O)O	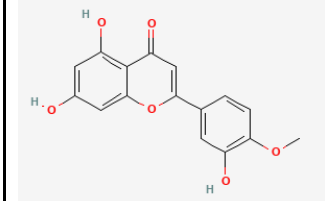
Ombuin (5320287)	*Cyperus teneriffae (nut grass)*	COC1=C(C=C(C=C1)C2=C(C(=O)C3=C(C=C(C=C3O2)OC)O)O)O	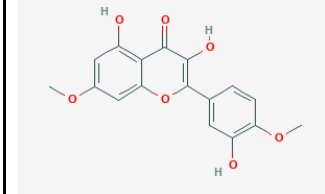

Baicalein (5281605)	*Scutellaria baicalensis and Scutellaria lateriflora*	C1=CC=C(C=C1)C2=CC(=O)C3=C(O2)C=C(C(=C3O)O)O	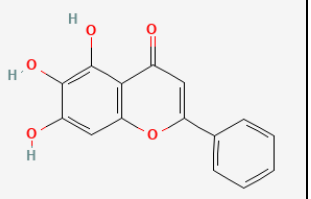
Chrysin (5281607)	*Passiflora caerulea (blue passionflower)*	C1=CC=C(C=C1)C2=CC(=O)C3=C(C=C(C=C3O2)O)O	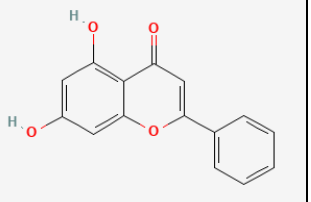
Cyanidin (128861)	*Glycine max (L.) Merr. (soybean)*	C1=CC(=C(C=C1C2=[O+]C3=CC(=CC(=C3C=C2O)O)O)O)O	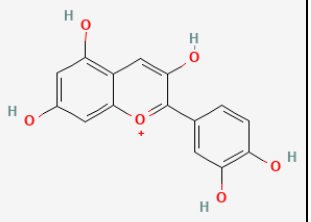
Iso-Rhamnetin (5281654)	*Opuntia ficus-indica (prickly pear)*	COC1=C(C=CC(=C1)C2=C(C(=O)C3=C(C=C(C=C3O2)O)O)O)O	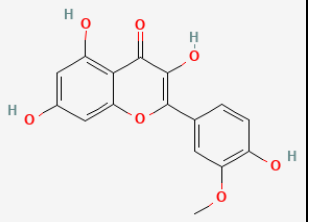
Shikonin (479503)	*Symphytum officinale L.(comfrey)*	CC(=CCC(C1=CC(=O)C2=C(C=CC(=C2C1=O)O)O)O)C	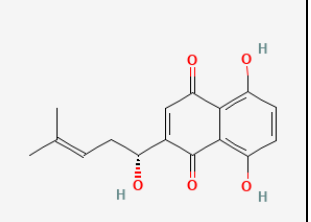

Okicamelliaside (10027940)	*Camellia japonica L*	C1OC2=C(O1)C3=C4C(=C2)C(=O)OC5=C4C(=CC(=C5O)OC6C(C(C(C(O6)CO)O)O)O)C(=O)O3	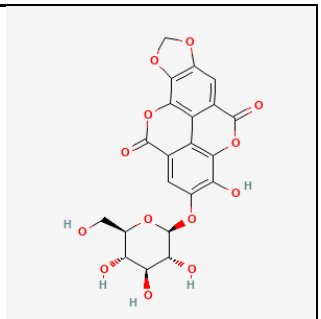
Warifteine (170074)	*Cissampelos sympodialis (milona)*	CN1CCC2=CC(=C(C3=C2C1CC4=CC=C(CO)C5=C(C=C6CCN=C(C6=C5O)CC7=CC=C(O3)C=C7)OC)C=C4)OOC.Cl.Cl	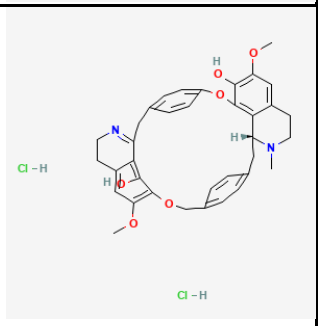
Methylwarifteine (102148214)	*Cissampelos sympodialis*	CN1CCC2=CC(=C(C3=C2C1CC4=CC(=CC=C4)OC5=C(C=C6CCNC(C6=C5)CC7=CC=C(O3)C=C7)OC)OC)OC	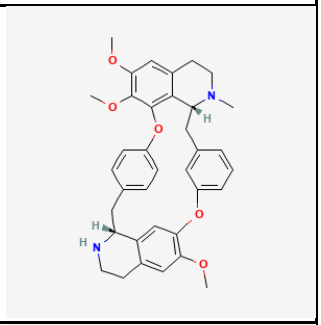
Luteolin-7-O Rutinoside (14032966)	*Mentha ×piperita L.*	C1=CC(=C(C=C1C2=CC(=O)C3=C(C=C(C=C3O2)OC4C(C(C(C(O4)COC5C(C(C(C(O5)CO)O)O)O)O)O)O)O)O)O	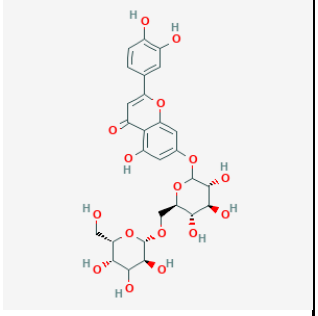
Tussilagone (13919185)	*Tussilago farfara L. (tussilago farfara)*	CCC(=CC(=O)OC1CC(C2C(C1=C)CC(=O)C2C(C)OC(=O)C)C(C)C)C	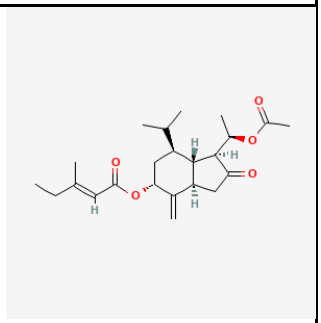

Petasin (5281526)	*Tephroseris palustris*	CC=C(C)C(=O)OC1CCC2=CC(=O)C(CC2(C1C)C)C(=C)C	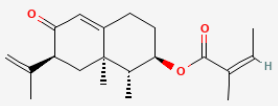
Mangiferin (5281647)	*Mangifera indica (mango)*	C1=C2C(=CC(=C1O)O)OC3=C(C2=O)C(=C(C(=C3)O)C4C(C(C(C(O4)CO)O)O)O)O	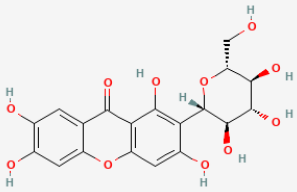
Scopoletin (5280460)	*Brachychiton rupestris (queenland bottle tree)*	COC1=C(C=C2C(=C1)C=CC(=O)O2)O	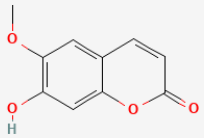
Sinomenine (5459308)	*Sinomenium acutum Rehd. et Wil*	CN1CCC23CC(=O)C(=CC2C1CC4=C3C(=C(C=C4)OC)O)OC	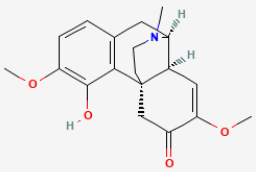
Emodin (3220)	*Reynoutria elliptica* (bamboo)	CC1=CC2=C(C(=C1)O)C(=O)C3=C(C2=O)C=C(C=C3O)O	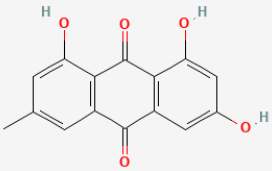

7-Epiclusianone (5471610)	*Garcinia brasiliensis Mart.*	CC(=CCC1CC2(C(=O)C(=C(C3=CC=CC=C3)O)C(=O)C(C2=O)(C1(C)C)CC=C(C)C)CC=C(C)C)C	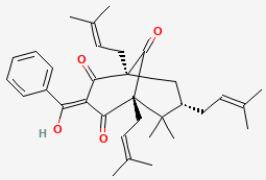
Anthopogochromae (46872460)	*Rhododendron anthopogonoides Maximowicz*	CC1=CC2=C(C3C(C4(C3C(O2)(CCC4)C)C)C(=O)CC(C)C)C(=C1C(=O)O)O	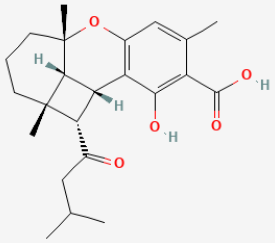
Schizandrin (23915)	*Schizandra chinensis*	CC1CC2=CC(=C(C(=C2C3=C(C(=C(C=C3CC1(C)O)OC)OC)OC)OC)OC)OC	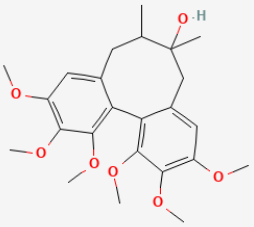
Diosgenin (99474)	*Dioscorea opposita thumb (Chinese yam)*	CC1CCC2(C(C3C(O2)CC4C3(CCC5C4CC=C6C5(CCC(C6)O)C)C)C)OC1	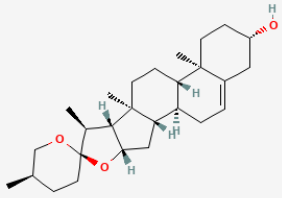
Valencene (9855795)	*Cyperus rotundus*	CC1CCC=C2C1(CC(CC2)C(=C)C)C	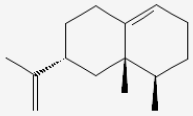

Piceatannol (667639)	*Cyperus longus*	C1=CC(=C(C=C1C=CC2=CC(=CC(=C2)O)O)O)O	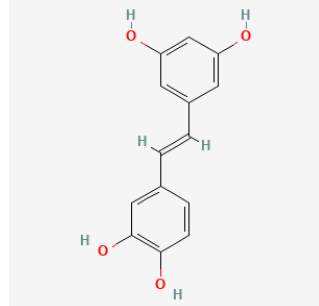
Amentoflavone (5281600)	*Hypericum perforatum L.*	C1=CC(=CC=C1C2=CC(=O)C3=C(O2)C(=C(C=C3O)O)C4=C(C=CC(=C4)C5=CC(=O)C6=C(C=C(C=C6O5)O)O)O)O	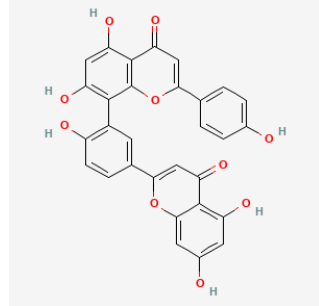
Glycyrrhiza (5317765)	Licorice (glycyrrhiza glabra)	CC1(C(CC2=C(O1)C=CC(=C2)C3=C(C(=O)C4=C(C=C(C=C4O3)O)O)O)O)O)C	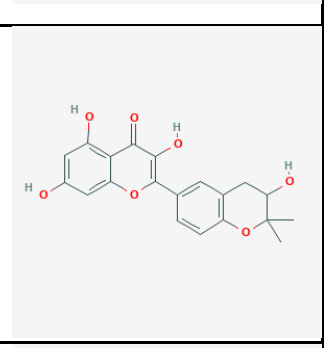
Isoliquiritin (5318591)	Licorice	C1=CC(=CC=C1C=CC(=O)C2=C(C=C(C=C2)O)O)OC3C(C(C(C(O3)CO)O)O)O)O	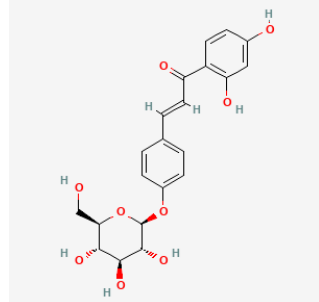
Liquiritigenin (114829)	licorice	C1C(OC2=C(C1=O)C=CC(=C2)O)C3=CC=C(C=C3)O	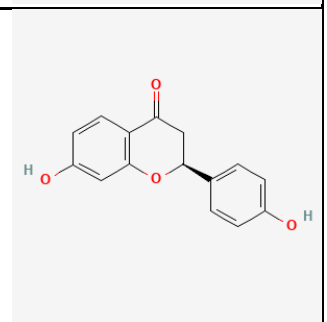

Ferulic Acid (445858)	Newbouldia laevis	COC1=C(C=CC(=C1)C=CC(=O)O)O	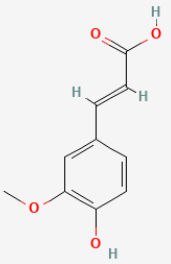
Vanillic Acid (8468)	Zea mays (Corn silk)	COC1=C(C=CC(=C1)C(=O)O)O	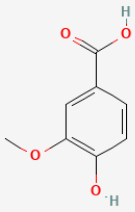
Para-Aminobenzoic Acid (978)	Zea mays	C1=CC(=CC=C1C(=O)O)N	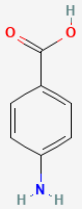
Chlorogenic Acid (1794427)	Zea mays	C1C(C(C(CC1(C(=O)O)O)OC(=O)C=CC2=CC(=C(C=C2)O)O)O)O	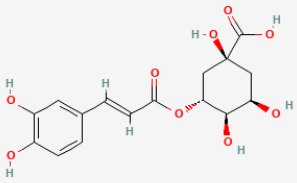
Protocatechuic Acid (72)	Zea mays	C1=CC(=C(C=C1C(=O)O)O)O	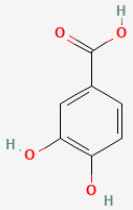

Hydroxycinnamic Acid Ester (637542)	Zea mays	C1=CC(=CC=C1C=CC(=O)O)O	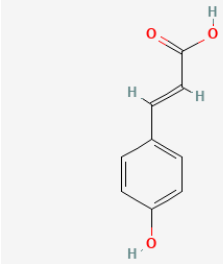
Fargesin (10926754)	*Schisandra chinensis*, *flos magnoliae liliflorae*, etc.	COC1=C(C=C(C=C1)C2C3COC(C3CO2)C4=CC5=C(C=C4)OCO5)OC	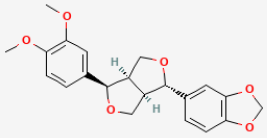
Tanshinone (114917)	*Paeonia lactiflora*, *Flos Farfarae*, the root of *Salvia miltiorrhiza*, etc.	CC1=C2C=CC3=C(C2=CC=C1)C(=O)C(=O)C4=C3OC=C4C	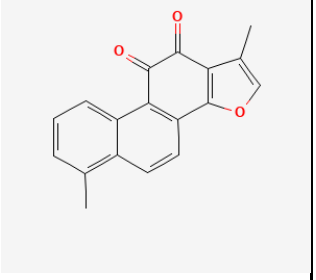
Oxymatrine (114850)	*Sophora flavescens*, *Chondrodendron tomentosum*, etc.	C1CC2C3CCC[N+]4(C3C(CCC4)CN2C(=O)C1)[O-]	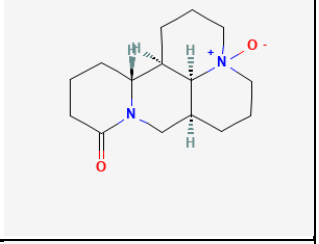
Curine (253793)	*Sophora flavescens*, *Chondrodendron tomentosum*, etc.	CN1CCC2=CC(=C3C=C2C1CC4=CC=C(C=C4)OC5=C6C(CC7=CC(=C(C=C7)O)O3)N(CCC6=CC(=C5O)OC)C)OC	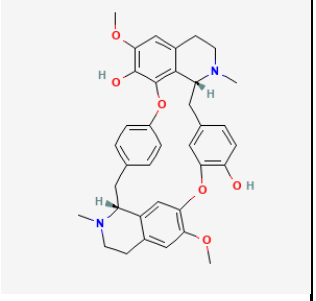

Matrine (91466)	*Sophora flavescens, Chondrodendron tomentosum*, etc.	C1CC2C3CCCN4C3C(CCC4)CN2C(=O)C1	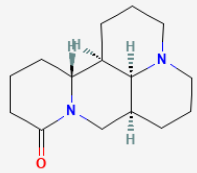
Lignans (44301)	*Schisandra chinensis, flos magnoliae liliflorae*, etc.	COC1=CC(=CC(=C1OC)OC)C2C3C(COC3=O)C(C4=CC5=C(C=C24)OCO5)O	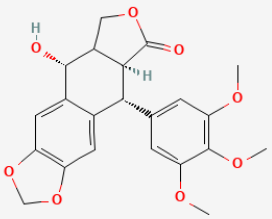

5.2. Screening of natural compounds through molecular docking:

Molecular docking constitutes a powerful computational method utilized to meticulously investigate the optimal intermolecular associations between a macromolecule and a small molecule, typically a drug compound via screening of chemical databases (Agu et al., 2023). It predicts which ligands will anticipate with a target to form the optimal complex. This methodological approach plays a pivotal role in the identification and assessment of potential lead compounds, thereby facilitating the discovery and development of innovative pharmaceutical agents. AutoDock vina software was used to determine intermolecular interactions between the selected target protein i.e. 3RZE and 110 novel natural compounds having bioactivity of anti-allergic properties through molecular docking. This study evaluated the binding free energy of each compound to identify potential candidates for further investigation. A protein-ligand complex with low binding energy generally signifies a strong binding affinity. Therefore, **Table 2** consist of 10 hit compounds with the most favourable binding energy (below -7.5 Kcal/mol) to the histamine H_1 receptor protein along with RMSD (Å) were selected as potential leads and visualised in PyMOL. The green sphere shape shows the target protein and the blue line shape shows the ligand.

Table 2: Molecular docking results

S.No.	Compound name	Docking Results (Affinity- Kcal/mol, RMSD- Å)	Docked Complex
1.	Fucofuroeckol-A	Affinity = -8.5 Rmsd (l.b) =3.950 Rmsd (u.b) =8.45	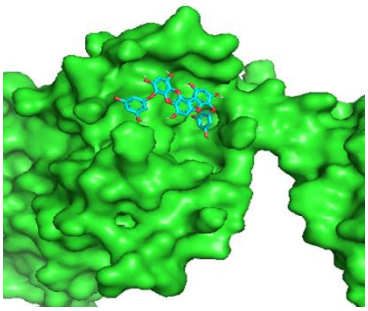
2.	Epigallocatechin gallate	Affinity = -7.8 Rmsd (l.b) =0.114 Rmsd (u.b) =2.051	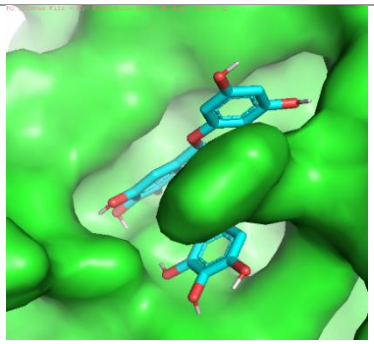
3.	Paucin	Affinity = -7.5 Rmsd (l.b) =2.149 Rmsd (u.b) =8.649	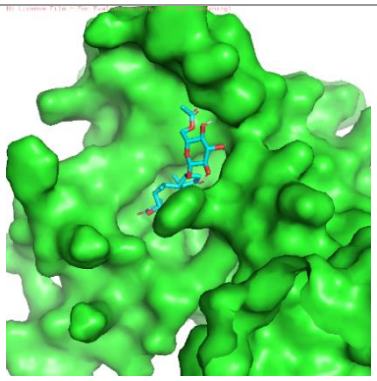
4.	Kenusanone A	Affinity =-7.5 Rmsd (l.b) =2.980 Rmsd (u.b) =3.895	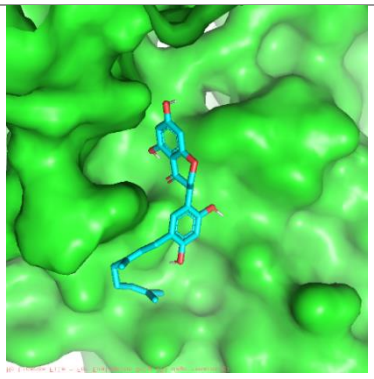

5.	Baicalin	Affinity =-8.2 Rmsd (l.b) =2.203 Rmsd (u.b) =4.007	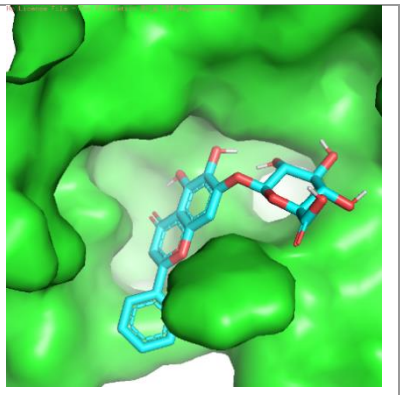
6.	Rutin	Affinity =-7.9 Rmsd (l.b) =12.439 Rmsd (u.b) =16.077	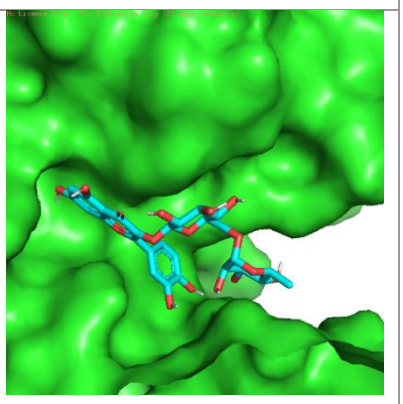
7.	Silymarin	Affinity =-8.0 Rmsd (l.b) =4.400 Rmsd (u.b) =10.509	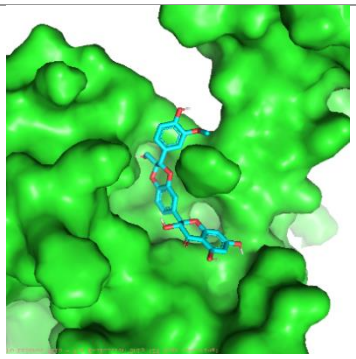
8.	Okicamelliaside	Affinity =-8.2 Rmsd (l.b) =1.964 Rmsd (u.b) =8.564	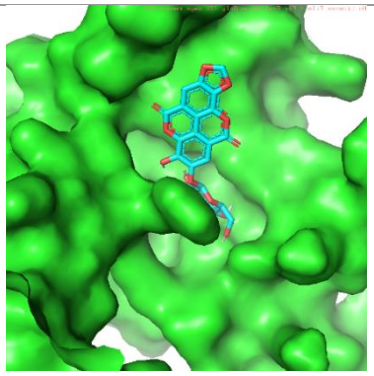

9.	luteolin-7-O-rutinoside	Affinity =-8.5 Rmsd (l.b) =4.981 Rmsd (u.b) =10.857	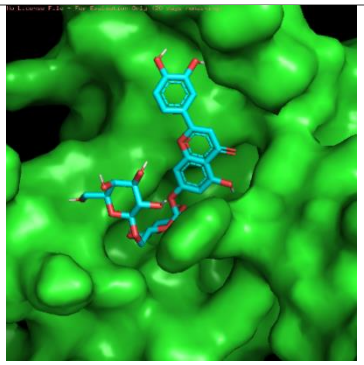
1(	Glycyrrhiza	Affinity =-8.0 Rmsd (l.b) =6.277 Rmsd (u.b) =8.284	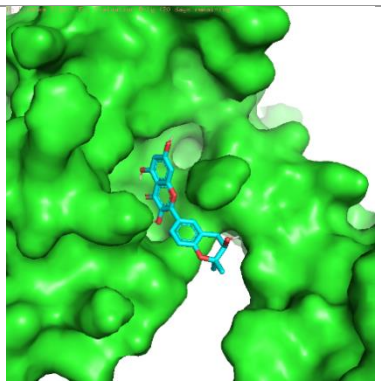

5.3. Interaction analysis:

BIOVIA Discovery Studio software was used to visualize the interaction between the selected compounds and human Histamine H_1 receptor. The ligand interacts with the receptor's amino acids through different bond type like pi-cation, amide-pi stacked, conventional hydrogen bond, pi-alkyl, alkyl, pi-sigma and pi-pi. **Table 3** shows the number of bonds, interacting amino acids, bond type, bond distance and 2D interaction of docked complexes.

Table 3: 2D interactions between amino acids and ligand along with type of bonds, no. of bonds and bond distance

Compound Name	No. Of Bonds	Type of Interactions			2D Structure
		Interacting amino acid	Bond type	Bond distance	
Baicalin	12	LYS A: 412	Pi – Cation	4.59	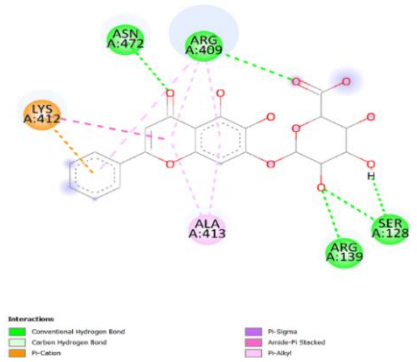
			Amide – Pi Stacked	5.39	
		ASN A: 472	Conventional Hydrogen bond	2.30	
		ARG A: 409	Pi – Alkyl	5.00, 4.44, 4.58	
			Conventional Hydrogen bond	2.32	
		ALA A: 413	Pi – Alkyl	4.49, 4.32	
		ARG A:139	Conventional Hydrogen bond	2.28	
		SER A:128	Conventional Hydrogen bond	2.32, 2.11	
Epigallocatechin gallate	10	GLU A: 410	Conventional Hydrogen bond	2.11	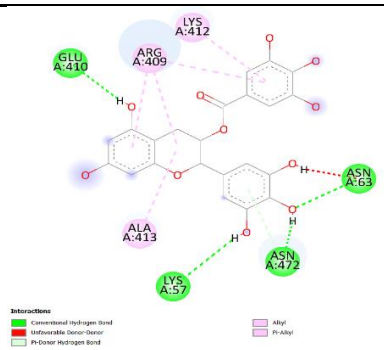
		LYS A: 57	Conventional Hydrogen bond	2.96	
		ASN A: 472	Conventional Hydrogen bond	2.14	
			Pi – donor hydrogen bond	2.93	
		ASN A: 63	Conventional Hydrogen bond	2.44	
		ALA A: 413	alkyl	4.93	
		ARG A: 409	Pi -Alkyl	4.00, 4.33, 5.09	
		LYS A: 412	alkyl	4.61	

glycyrrhiza	13	ALA A: 413	Alkyl, Pi-Alkyl	4.78, 4.58	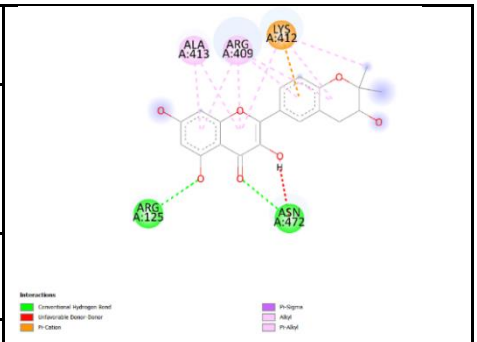
		ARG A: 409	Alkyl, Pi-Alkyl	4.76, 4.43, 4.83, 5.38	
		ARG A: 125	Conventional Hydrogen bond	2.60	
		ASN A: 472	Conventional Hydrogen bond	2.58	
		LYS A: 412	Alkyl, Pi-Alkyl	5.35, 4.73, 4.11, 4.47	
			Pi -cation	4.73	
Kenusanone A	9	LEU A: 207	Alkyl	3.88	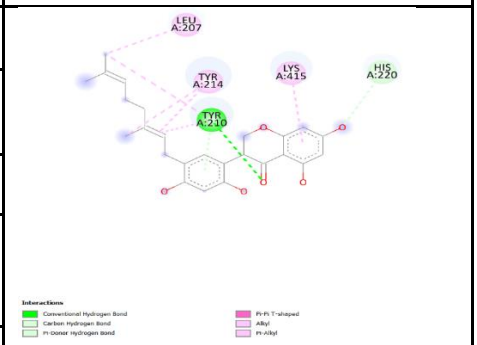
		TYR A:214	Alkyl	4.05, 3.72	
		LYS A: 415	Alkyl	4.00	
		HIS A: 220	Carbon Hydrogen Bond	3.19	
		TYR A: 210	Carbon Hydrogen Bond	2.69	
			Conventional Hydrogen bond	2.44	
			Alkyl	5.19, 4.88	
Luteolin-7-O-rutinoside	9	ASN A: 63	Conventional Hydrogen bond	2.48, 2.58	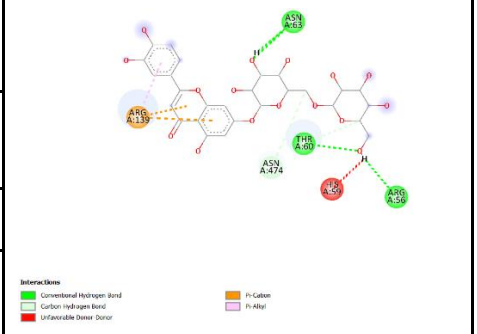
		ARG A: 139	Pi – Cation	3.52, 3.62	
			Pi - Alkyl	3.68	
		ASN A: 474	Carbon Hydrogen Bond	3.34	
		THR A:60	Conventional Hydrogen bond	2.75	
			Carbon Hydrogen	3.25	

			Bond		
		ARG A:56	Conventional Hydrogen bond	2.65	
Okicamelliaside	12	ASN A: 474	Conventional Hydrogen bond	2.74	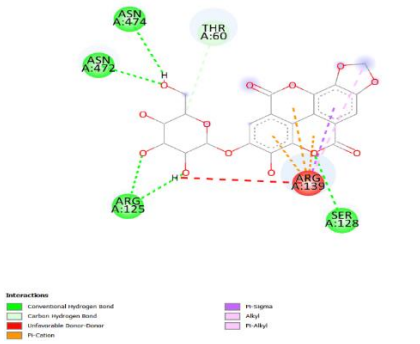
		ASN A: 472	Conventional Hydrogen bond	2.14	
		ARG A: 125	Conventional Hydrogen bond	2.24, 2.45	
		SER A: 128	Conventional Hydrogen bond	2.97	
		THR A: 60	Carbon Hydrogen Bond	3.52	
		ARG A: 139	Unfavorable donor- donor	2.62	
			Pi – cation	3.58, 3.40, 4.52	
			Pi - sigma	3.57	
			alkyl	4.10	
Paucin	6	ASN A: 63	Conventional Hydrogen bond	2.41	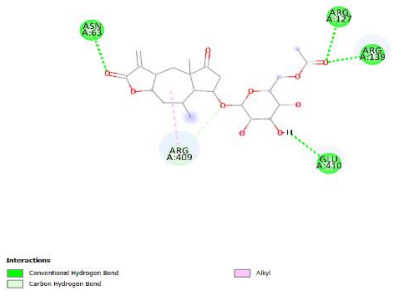
		ARG A: 409	Alkyl	5.13	
			Carbon Hydrogen Bond	3.28	
		GLU A: 410	Conventional Hydrogen bond	2.59	
		ARG A: 139	Conventional Hydrogen bond	2.26	
		ARG A: 127	Conventional Hydrogen bond	2.47	
Rutin	8	ALA A: 414	Amide – Pi stacked	4.54	

		LYS A: 415	Pi - Alkyl	4.34, 3.86	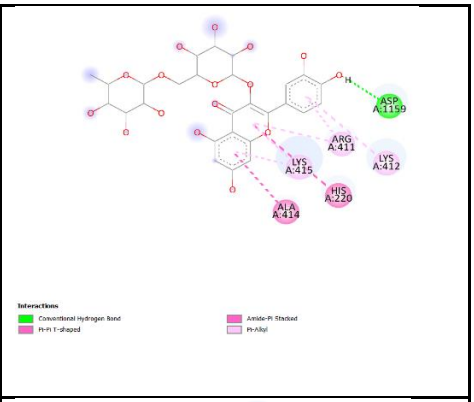
		HIS A: 220	Pi – Pi	5.30	
		ARG A: 411	Pi - Alkyl	5.48, 3.86	
		LYS A: 412	Pi - Alkyl	5.32	
		ASP A: 1159	Conventional Hydrogen bond	1.91	
Silymarin	8	ALA A: 413	Pi – sigma	3.96	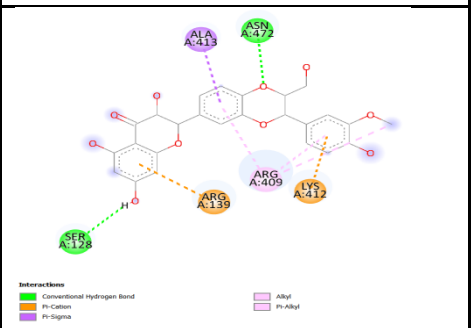
		ASN A: 472	Conventional Hydrogen bond	2.49	
		SER A: 128	Conventional Hydrogen bond	2.45	
		ARG A: 409	Alkyl	4.89, 5.00, 3.98	
		ARG A: 139	Pi – cation	4.30	
		LYS A: 412	Pi – cation	4.60	
Fucofuroeckol A	7	ARG A: 139	Pi – cation	6.13	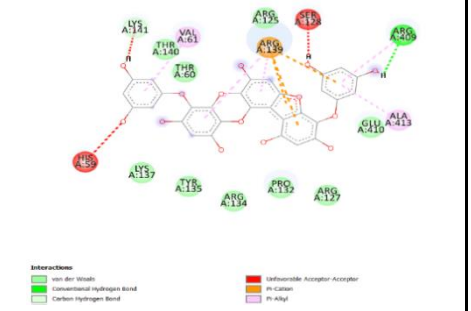
		ARG A: 409	Conventional hydrogen bond	5.45	
		VAL A: 61	Pi - alkyl	5.77	
		ALA A: 413	Pi - alkyl	6.55	
		HIS A: 59	Unfavorable bond	6.34	
		SER A: 128	Unfavorable bond	3.71	
		LYS A: 141	Carbon hydrogen bond	3.32	

5.4. Assessment of drug-likeness through PAINS analysis:

The term PAINS (pan-assay interference compounds) has been coined to describe seemingly bioactive molecules that can disrupt readouts by interacting with unrelated biological targets or testing methods (Baell & Nissink, 2018). So, the software DruLiTo is used to filter out screened compounds on the basis of molecular properties like molecular weight, partition coefficient, hydrogen bond acceptor, hydrogen bond donor, no. of rings, no. of rigid bond, molar refractivity and no. of atoms. The molsoft tool was used to predict the drug-likeness score and graph. Table 4 shows the molecular filters used and the drug-likeness score along with the graph.

Table 4: Prediction of physiochemical parameters along with drug likeness score and graph (Lipinski's rule (no. of HBD<5, no. of HBA <10, molecular weight <500 and ClogP<5), Molecular Detection of Drug Resistance (no. of rings >3, no. of rigid bonds >18 and no. of rotatable bonds >6), Ghose rule (logP, molar refractivity, molecular weight, no. of atoms and polar surface area < 140)

Compound	Lipinski's rule	MDDR	Ghose	Summary	Score and graph
Baicalin	MW-446.08 LogP-1.051 HBA- 11 HBD- 6	nRB- 4 RC- 4 nRigidB-31	AMR-112.72 nAtom-50	Pass ghose filter only	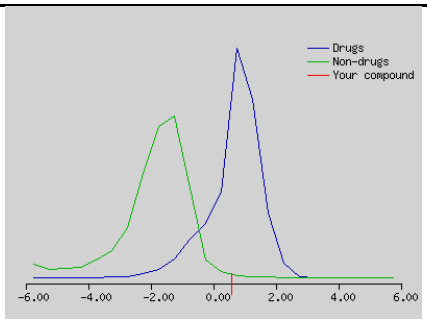 **Drug-likeness model score:** 0.58
Epigallocatechin gallate	MW-458.08 LogP-2.984 HBA-11 HBD-8	nRB- 4 RC- 4 nRigidB-32	AMR-120.95 nAtom-51	Pass ghose filter only	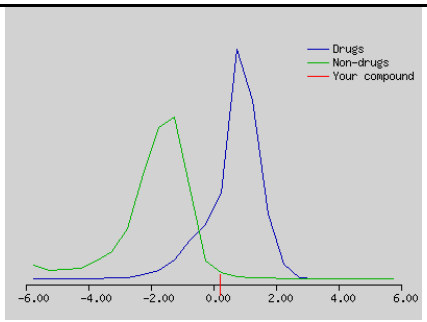 **Drug-likeness model score:** 0.23

Fucofuroeckol-A	MW-772.13 LogP-4.224 HBA-18 HBD-0	nRB- 16 RC- 6 nRigidB-45	AMR-199.79 nAtom-84	Pass MDDR rule only	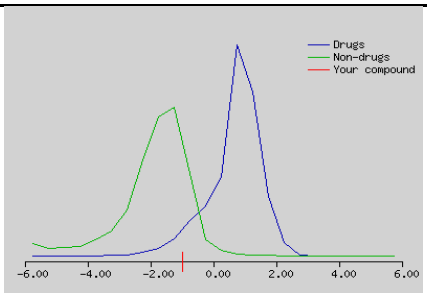 **Drug-likeness model score:** -1.00
Glycyrrhiza	MW-370.11 LogP-1.813 HBA-7 HBD- 4	nRB- 1 RC-4 nRigidB-29	AMR-104.55 nAtom-45	Violate only MDDR rule	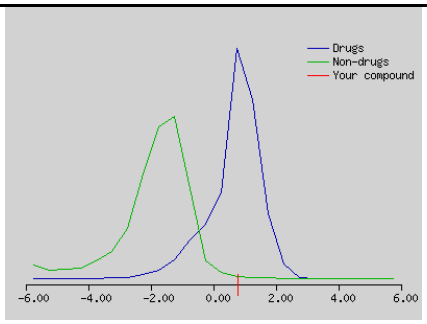 **Drug-likeness model score:** 0.79
Kenusanone A	MW-424.19 LogP-3.831 HBA-6 HBD-4	nRB- 6 RC-3 nRigidB-27	AMR-128.07 nAtom-59	Pass all the rule	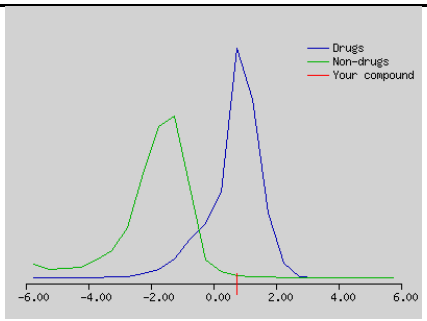 **Drug-likeness model score:** 0.75
luteolin-7-O-rutinoside	MW-610.15 LogP—1.357 HBA-16 HBD-10	nRB- 7 RC- 5 nRigidB-40	AMR-146.87 nAtom-73	Pass MDDR rule only	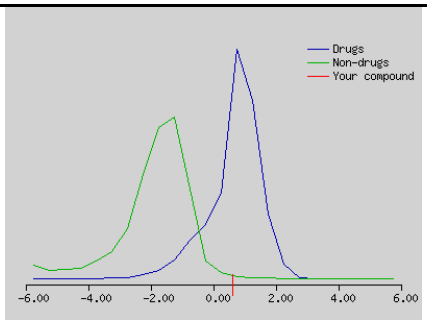 **Drug-likeness model score:** 0.61
Okicamelliaside	MW-476.06 LogP—0.229 HBA- 13 HBD-5	nRB- 3 RC-6 nRigidB-36	AMR-110.31 nAtom-50	Pass only ghose filter	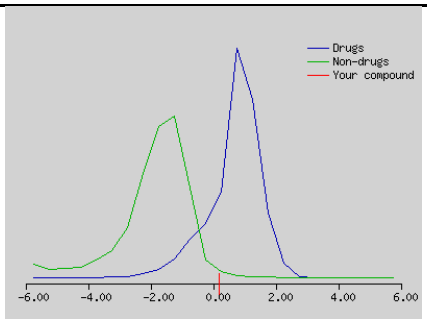

					Drug-likeness model score: 0.19
Paucin	MW-468.2 LogP—1.095 HBA-10 HBD-3	nRB- 5 RC-4 nRigidB-31	AMR-108.28 nAtom-65	Pass Lipinski and ghose rule	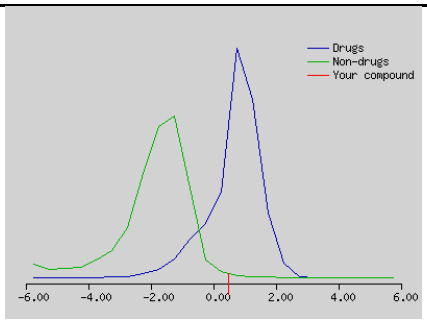 **Drug-likeness model score:** 0.48
Rutin	MW-610.15 LogP—0.735 HBA-16 HBD-10	nRB- 6 RC-5 nRigidB-41	AMR-147.17 nAtom-73	Pass only MDDR rule	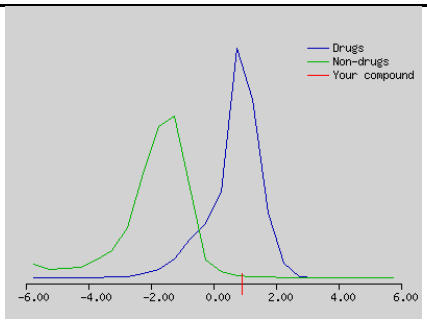 **Drug-likeness model score:** 0.91
Silymarin	MW-482.12 LogP-0.855 HBA-10 HBD-5	nRB- 4 RC-5 nRigidB-35	AMR-132.21 nAtom-57	Pass only Lipinski rule	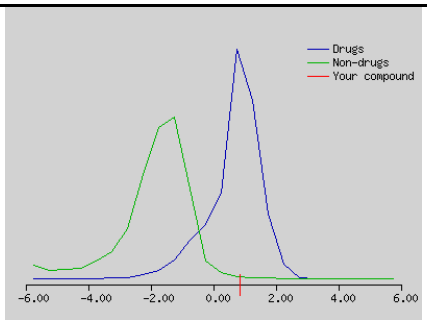 **Drug-likeness model score:** 0.84

5.5. ADMET analysis:

The ADMET evaluation completed using ADMETlab 2.0 has provided a comprehensive prediction of the target molecule's physicochemical, medicinal chemistry, ADME, and toxicity properties. This data offers significant insights into the molecule's capacity for absorption, distribution, metabolism, excretion, and potential toxicological effects. **Table 5 shows** the prediction probability values of ADMET that are transformed into six symbols: 0-0.1(---), 0.1-0.3(--), 0.3-0.5(-), 0.5-0.7(+), 0.7-0.9(++), and 0.9-1.0(+++)

Table 5 shows the pharmacokinetic parameters of lead compounds

Compound	Absorption				Distribution			
	caco-2 permeability	MDCK Permeability	Pgp - inhibitor	HIA	PPB	VD	BBB Penetration	Fu
Fucofuroeckol-A	-5.260	1.9e-05	+++	+++	82.428 %	0.674	- - -	21.310%
Epigallocatechin gallate	-6.608	4.6e-06	- - -	+++	87.879 %	0.521	- - -	8.260%
Paucin	-5.236	9.9e-05	- - -	+++	33.644 %	0.422	- -	64.338%
Kenusanone A	-4.933	1.2e-05	-	- - -	99.404 %	0.956	- - -	0.931%
Baicalin	-6.340	2.2e-05	- - -	++	83.360 %	0.591	- - -	11.347%
Rutin	-6.336	3e-05	- - -	+++	83.811 %	0.754	- -	20.866%
Silymarin	-6.255	9.5e-06	-	-	96.657 %	0.649	- - -	5.734%
Okicamelliaside	-6.139	4.6e-05	- - -	+	67.666 %	1.063	- - -	23.806%
luteolin-7-O-rutinoside	-6.343	9.2e-05	- - -	+++	78.970 %	0.577	-	21.330%
Glycyrrhiza	-5.031	1.1e-05	- - -	- - -	98.336 %	0.564	- - -	3.550%

Compound	Metabolism								Excretion	
	CYP1A2 inhibitor	CYP2C19 inhibitor	CYP2C9 inhibitor	CYP2C9 substrate	CYP2D6 inhibitor	CYP2D6 substrate	CYP3A4 inhibitor	CYP3A4 substrate	CL	T ½
Fucofuroeckol-A	- -	-	+	+	- - -	- - -	- -	- -	1.020	0.291
Epigallocatechin gallate	- -	- - -	+	- -	- - -	- -	- - -	- -	16.556	0.928
Paucin	- - -	- - -	- - -	- -	- - -	- -	- - -	- -	2.720	0.340
Kenusanone A	+++	+++	++	+++	+++	++	+	- -	14.571	0.364
Baicalin	- - -	- - -	- - -	- -	- - -	- -	- - -	- - -	1.000	0.855
Rutin	- - -	- - -	- - -	- -	- - -	- -	- - -	- - -	1.349	0.524
Silymarin	- - -	- -	+	++	-	-	++	-	5.144	0.274
Okicamelliaside	- - -	- - -	- - -	- -	- - -	- -	- -	- - -	1.722	0.311
luteolin-7-O-rutinoside	- - -	- - -	- - -	- -	- - -	- -	- - -	- - -	1.314	0.443
Glycyrrhiza	+ +	- -	++	++	+	- -	-	- -	5.722	0.693

Compound	Toxicity										
	hERG blockers	H-HT	DILI	AMES Toxicity	Rat oral acute toxicity	FDAMDD	Skin sensitization	carcinogenicity	Eye corrosion	Eye irritation	Respiratory toxicity
Fucofuroeckol-A	---	---	+	---	+++	+++	+++	---	--	+++	--
Epigallocatechin gallate	--	--	+++	--	---	--	+++	---	---	+++	---
Paucin	---	--	+	--	+	---	---	--	---	---	---
Kenusanone A	---	-	+	--	-	++	+++	--	---	++	--
Baicalin	---	--	+++	---	---	---	---	--	---	---	---
Rutin	---	---	+++	++	---	---	---	---	---	---	---
Silymarin	---	---	+++	-	--	---	--	-	---	--	---
Okicamelliaside	---	+ +	+++	--	---	---	--	++	---	---	---
luteolin-7-O-rutinoside	---	---	+++	+	---	---	---	-	---	---	---
Glycyrrhiza	---	--	+++	-	--	+ +	-	--	---	--	--

Compound	Toxicophore Rule			
	Acute toxicity rule	**Genotoxic carcinogenicity rule**	**Non-genotoxic carcinogenicity rule**	**FAF- drugs4 rule**
Fucofuroeckol-A	0 alert	3 alerts	1 alert	1 alert
Epigallocatechin gallate	0 alert	0 alert	0 alert	2 alerts
Paucin	0 alert	1 alert	0 alert	1 alert
Kenusanone A	0 alert	0 alert	0 alert	1 alert
Baicalin	0 alert	0 alert	0 alert	2 alerts
Rutin	0 alert	0 alert	0 alert	2 alerts
Silymarin	0 alert	0 alert	0 alert	1 alert
Okicamelliaside	0 alert	5 alerts	2 alerts	3 alerts
luteolin-7-O-rutinoside	0 alert	0 alert	0 alert	2 alerts
Glycyrrhiza	0 alert	0 alert	0 alert	1 alert

5.6. Bioacticity Score:

The Molinspiration bioactivity score determines the drug-likeness of active compounds based on various factors such as ion channel modulators, kinase inhibitors, GPCR ligands, nuclear receptor ligands, protease inhibitors, and other enzyme inhibitors(Khan et al., 2017). Utilising a dataset consisting of more than 100,000 typical drug molecules, this score facilitates effective discrimination between active and inactive compounds. The lead compounds were filtered out therefore, kenusanone A, silymarin, glycyrrhiza and paucin were the selected compound because they pass Lipinski's rule and other toxicity tests. **Table 6** predicts the bioactivity score of selected lead compounds with the help of molinspiration.

Table 6: Bioactivity score prediction

Bioactivity score	**Compounds**		
	Kenusanone A	Silymarin	Glycyrrhiza
GPCR ligand	0.08	0.07	0.08
Ion channel modulator	-0.00	-0.05	0.04
Kinase inhibitor	-0.06	0.01	0.14
Nuclear receptor ligand	0.63	0.16	0.61
Protease inhibitor	-0.13	0.02	0.04
Enzyme inhibitor	0.44	0.23	0.45

5.7. Conformational and structural analysis during MD Simulation:

Molecular dynamics (MD) simulations were important for validating the stability of proteins along with their interactions with ligands. 100ns molecular dynamic simulation was performed to observe the dynamic behavior of the 3RZE protein in both unbound and bound states, before and after ligand binding. Multiple parameters, such as RMSD (Root Mean Square Deviation), Rg (Radius of Gyration), RMSF (Root Mean Square Fluctuation), SASA (Solvent Accessible Surface Area), PCA (Principal Component Analysis), H-bond distribution, no. of h-bond (Hydrogen Bond), and conformation at different time intervals. The results were summarised using the binding free energy calculation.

5.7.1. Stability Analysis:

To explore the stability of selected compounds with histamine H_1 receptor, root mean square deviation (RMSD) quantifies the disparities in the protein's backbone structure with final conformations in 100ns environment. It assessed the root mean square deviation for both the protein (backbone) and the protein-ligand complex (complex). The findings demonstrated consistent root mean square deviation values with slight variations. **Figure 2** depicts the protein-ligand structural steadiness. Throughout the simulation, the backbone and the complex exhibited stability with slight fluctuations.

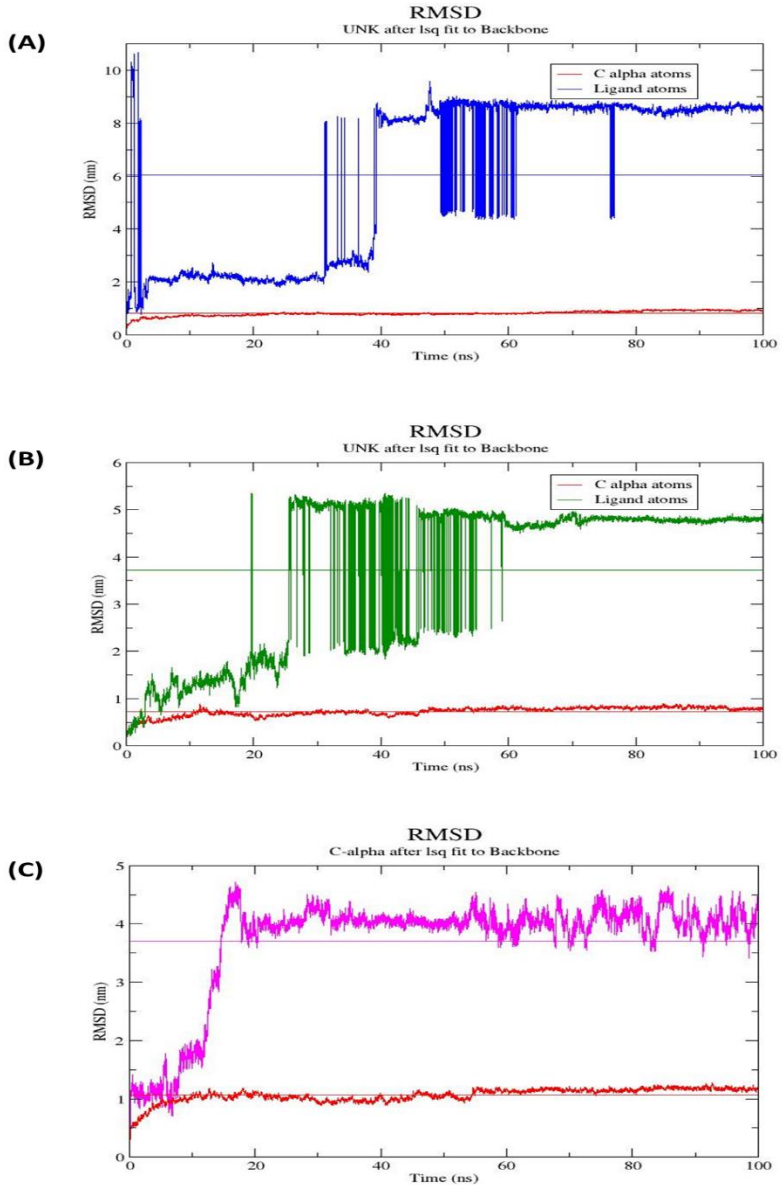

Figure 2: (A), (B) and (C) shows the RMSD evolution for the selected compound silymarin (blue), glycyrrhiza (green) and kenusanone A (pink) with protein (red) during 100ns MD simulation

5.7.2. Flexibility Analysis:

Flexibility is a key factor in maintaining the properties of proteins, and it can be evaluated by conducting RMSF analysis. Hence, the root means square fluctuation (RMSF) of the 3RZE protease and its complexes was examined during the final 100 ns of the stabilised trajectory. This analysis demonstrates the variability of amino acid residues when a ligand binds, revealing that residue in positions 200 to 300 exhibit greater fluctuations than residues in positions 1 to 199. Meanwhile, there was minimal variation observed in **figure 3**(A) which showed less fluctuation (value is under 0.6nm) means rigid and stabilized after binding. This finding further confirms their potential as promising compounds.

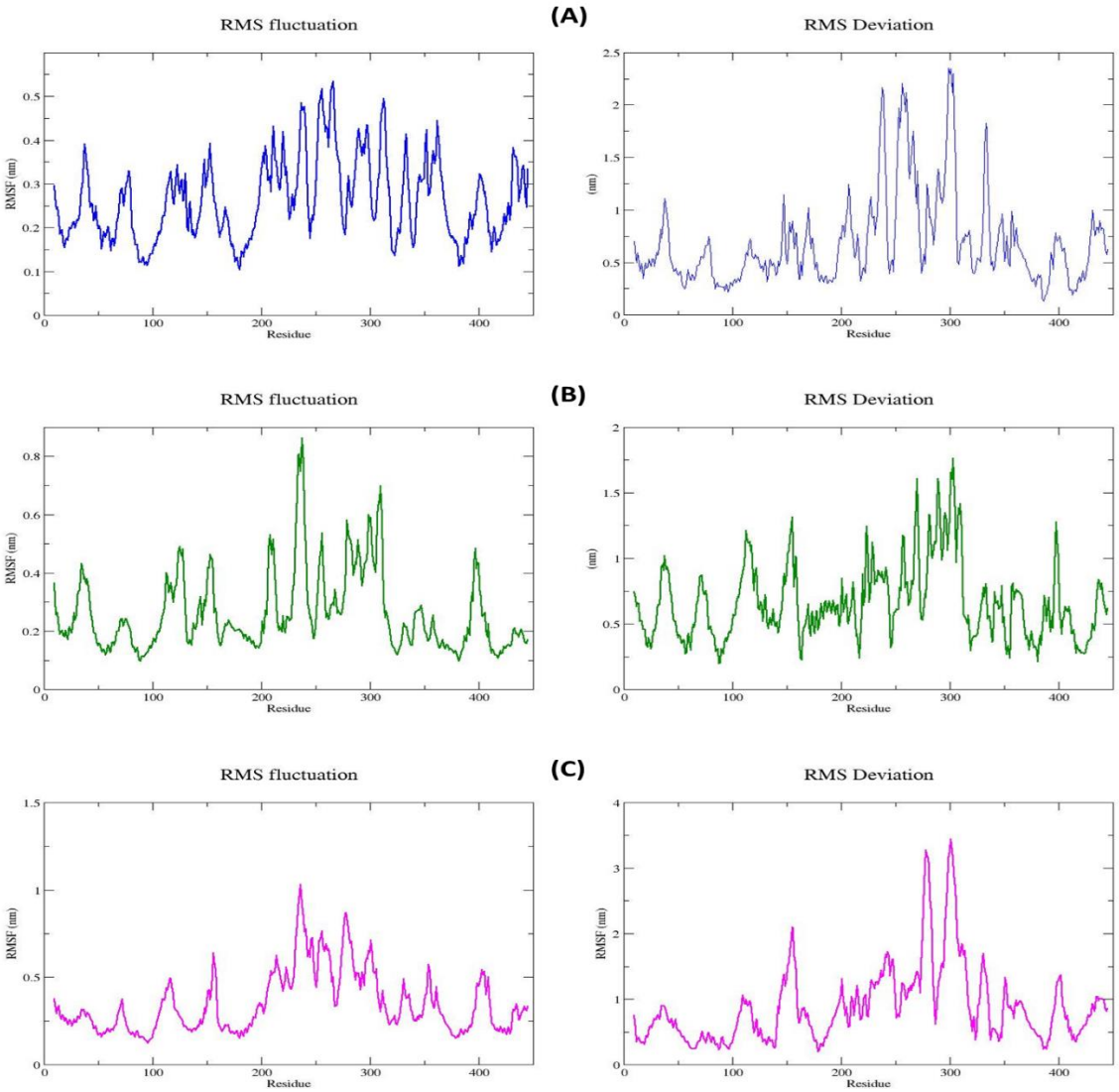

Figure 3: (A), (B) and (C) shows the RMSF evolution and RMSD of residues for the selected compound silymarin (blue), glycyrrhiza (green) and kenusanone A (pink) during 100ns MD simulation

5.7.3. Compactness analysis:

To evaluate the protein folding, stability and compactness, the radius of gyration (Rg) values was used to calculate over the time. The 3RZE protein and their complexes were evaluated for Rg values to validate their structural compactness. In **Figure 4,** the Rg values of the 3RZE protein with the selected compounds were plotted and calculated from the final 100 ns trajectories. The average Rg values were 3.2nm, 2.9nm and 3.1nm of silymarin (blue), glycyrrhiza (green) and kenusanone A (pink) respectively. The Rg results indicate that 3RZE with silymarin and kenusanone A exhibits more compact structure than glycyrrhiza.

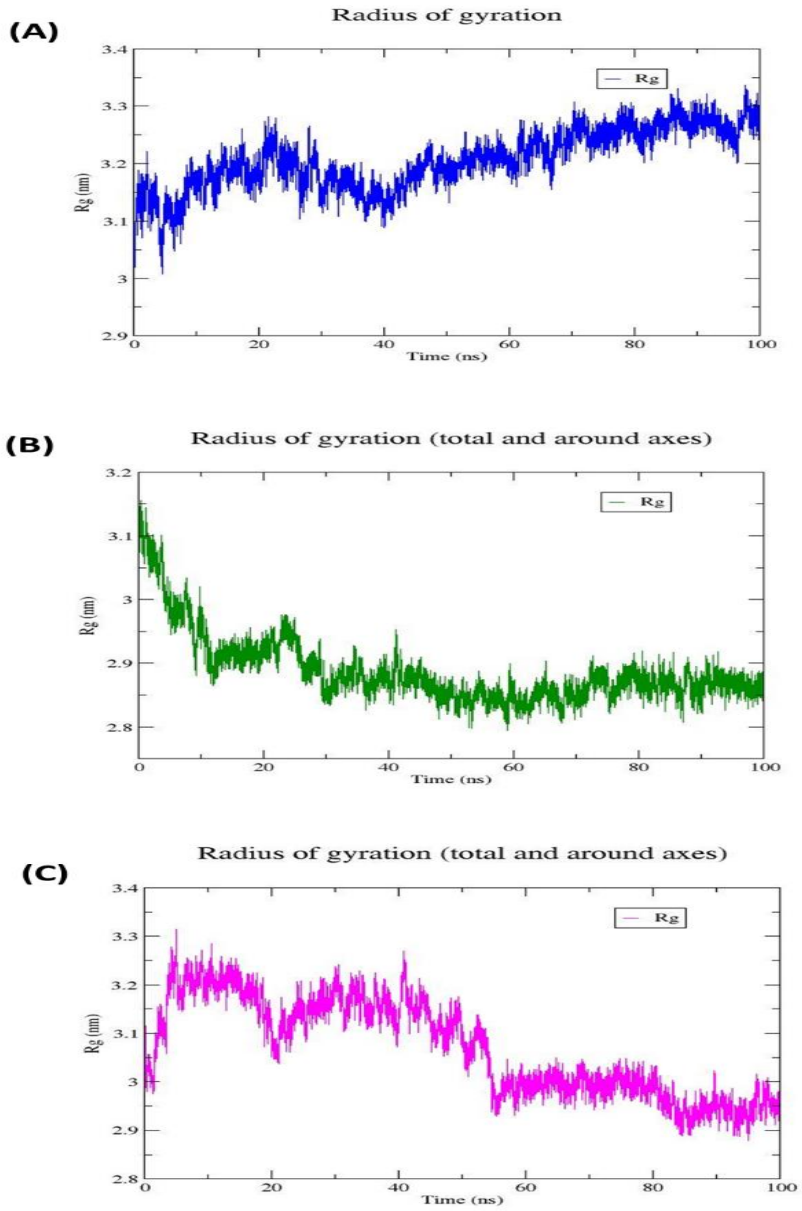

Figure 4: (A), (B) and (C) shows the radius of gyration (Rg) plots of selected compound silymarin (blue), glycyrrhiza (green) and kenusanone A (pink) during 100ns MD simulation

5.7.4. Solvent Accessible Surface Area (SASA) Analysis:

Solvent Accessible Surface Area (SASA) measures the proportion of a protein's surface that can be further accessible by solvent molecules. This metric has significance for interpreting various molecular phenomena, such as conformational changes, protein-ligand binding occurrences, and protein interactions. Through the analysis of the SASA, we have gained insight into how a protein's structure undergoes alterations in reaction to its surroundings or interactions with other molecules. The SASA values were calculated during the simulation using the "gmx sasa" tool. In **Figure 5** the obtained data were utilised to create comparative graphs that visually illustrate the changes in surface area over the final 100ns simulation.

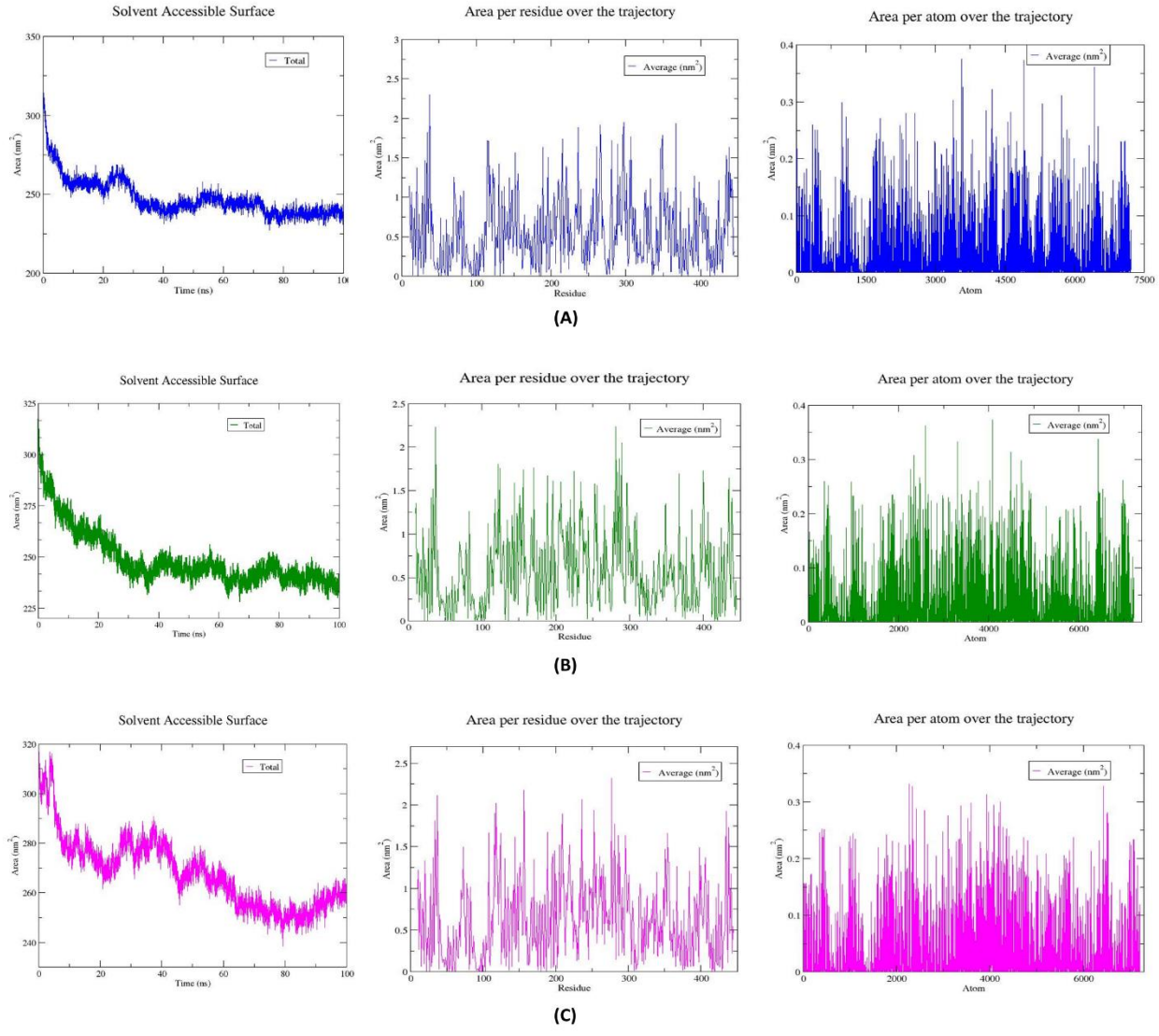

Figure 5: (A), (B) and (C) shows the Solvent Accessible Surface Area (SASA) plots of selected compound silymarin (blue), glycyrrhiza (green) and kenusanone A (pink) respectively during 100ns MD simulation

5.7.5. Hydrogen Bond Analysis:

Hydrogen bonds (HBs) play a vital part in facilitating the binding of ligands to target proteins. These bonds play a crucial role in stabilising the interactions between proteins and ligands, making them a pivotal factor in the design and effectiveness of compound. The study involved measuring the number of hydrogen bonds that formed between natural compounds and the target protein 3RZE. **Figure 6** plots the analysis that provides insight into the strength and durability of these interactions by No. of hydrogen bond and distribution of hydrogen bond, which are crucial for the efficacy of potential therapeutic agents. Furthermore, monitoring the quantity of hydrogen bonds offers valuable information about the strength of binding and how the compounds interact.

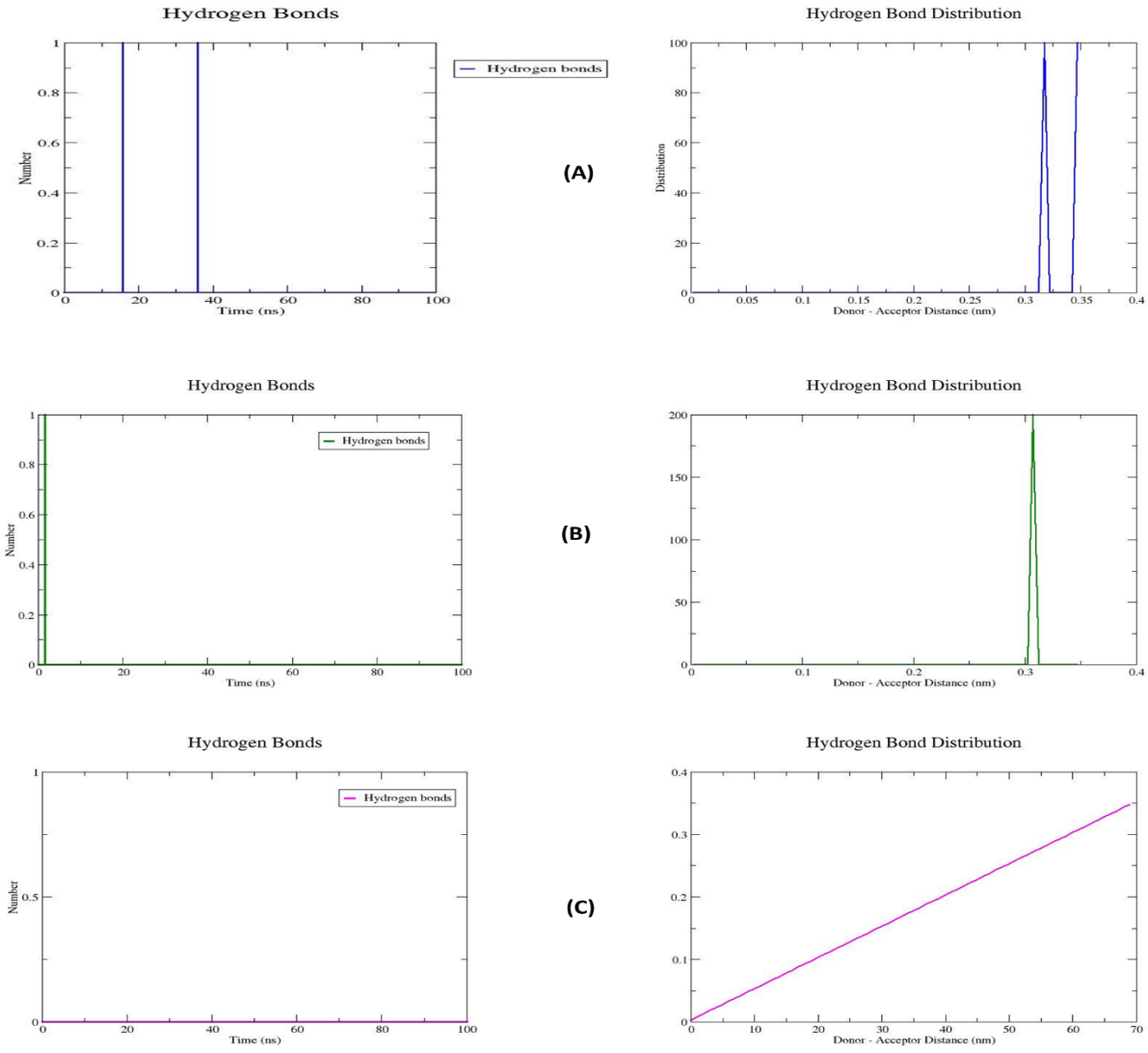

Figure 6: (A), (B) and (C) shows the number and distribution of hydrogen bonds plots of selected compound silymarin (blue), glycyrrhiza (green) and kenusanone A (pink) respectively during 100ns MD simulation

5.7.6. Principal Component Analysis (PCA):

Principal Component Analysis (PCA) was used to detect the primary movements that take place during the binding of a ligand with the protein. The analysis entailed the computation of eigenvectors and eigenvalues via matrix diagonalization. In order to evaluate the alterations in structural movement, our attention was directed towards the initial eigenvectors. The overall movement of a protein is mainly influenced by its dominant eigenvectors. This method enables us to precisely identify particular areas and forms of movement within the protein that are most influenced by the interaction with the ligand. Principal Component Analysis (PCA) was also used to create 2D projection plots of first few eigenvectors reflecting dynamics of the overall protein in **Figure 7.**

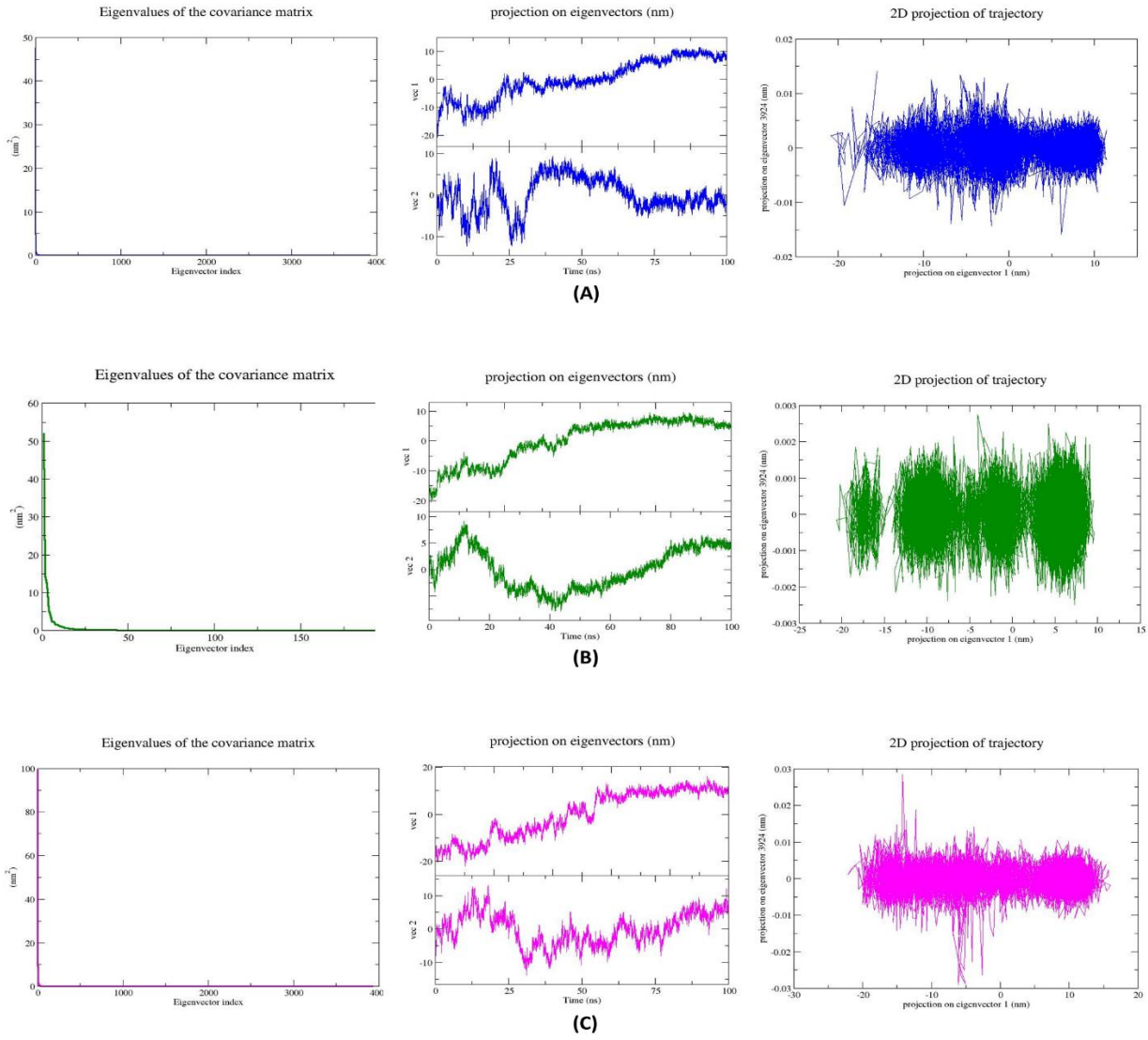

Figure 7: (A), (B) and (C) shows Plots of eigenvalues and the first few eigenvectors representing the motion of selected compound silymarin (blue), glycyrrhiza (green) and kenusanone A (pink) respectively during 100ns MD simulation

5.7.7. Energy Analysis:

The potential energy, kinetic energy, conserved energy, total energy, temperature and pressure of the 3RZE protein and the selected compounds in complex form was calculated. An error estimate of the average is given based on a block average over 5 blocks using the full-precision averages. Table 7 shows potential, kinetic, conserved and total energies along with temperature and pressure of the protein ligand complex.

Table 7: Energy analysis in 100ns MD simulation

Energy		**Lead Compounds**		
		Silymarin	**Glycyrrhiza**	**Kenusanone A**
Potential energy (kJ/mol)	**Average + error estimate**	-1.15817e ±110	-938998±93	-940171±80
	RMSD	1237.68	1116.67	1118.88
Kinetic energy (kJ/mol)	**Average + error estimate**	225863±1.1	184863±1.3	184838±1.2
	RMSD	830.491	757.773	758.182
Conserved energy (kJ/mol)	**Average + error estimate**	-221072±20000	-109907±18000	-110057±18000
	RMSD	407835	372406	369499
Total energy (kJ/mol)	**Average + error estimate**	-932306±110	-754134±93	-755333±79
	RMSD	1602.92	1457.25	1460.04
Temperature (K)	**Average + error estimate**	300.001±0.0014	300.005±0.0021	299.999±0.0019
	RMSD	1.10309	1.22975	1.23056
Pressure (bar)	**Average + error estimate**	0.929805±0.088	1.92665±0.47	1.11491±0.12
	RMSD	90.9878	105.03	104.98

5.7.8. Conformation Trajectories:

The conformation (gmx trjconv) can convert trajectory files into number of time frame with the different time stamp. In **Figure 8 (A)** the blue colour indicates the silymarin compound in 0ns, 20ns,40ns, 60ns, 80ns, 100ns respectively in the system of MD simulation. **(B)** the green colour indicates the glycyrrhiza compound in 0ns, 20ns,40ns, 60ns, 80ns, 100ns respectively in the system of MD simulation. **(C)** the pink colour indicates the kenusanone A compound in 0ns, 20ns,40ns, 60ns, 80ns, 100ns respectively in the system of MD simulation.

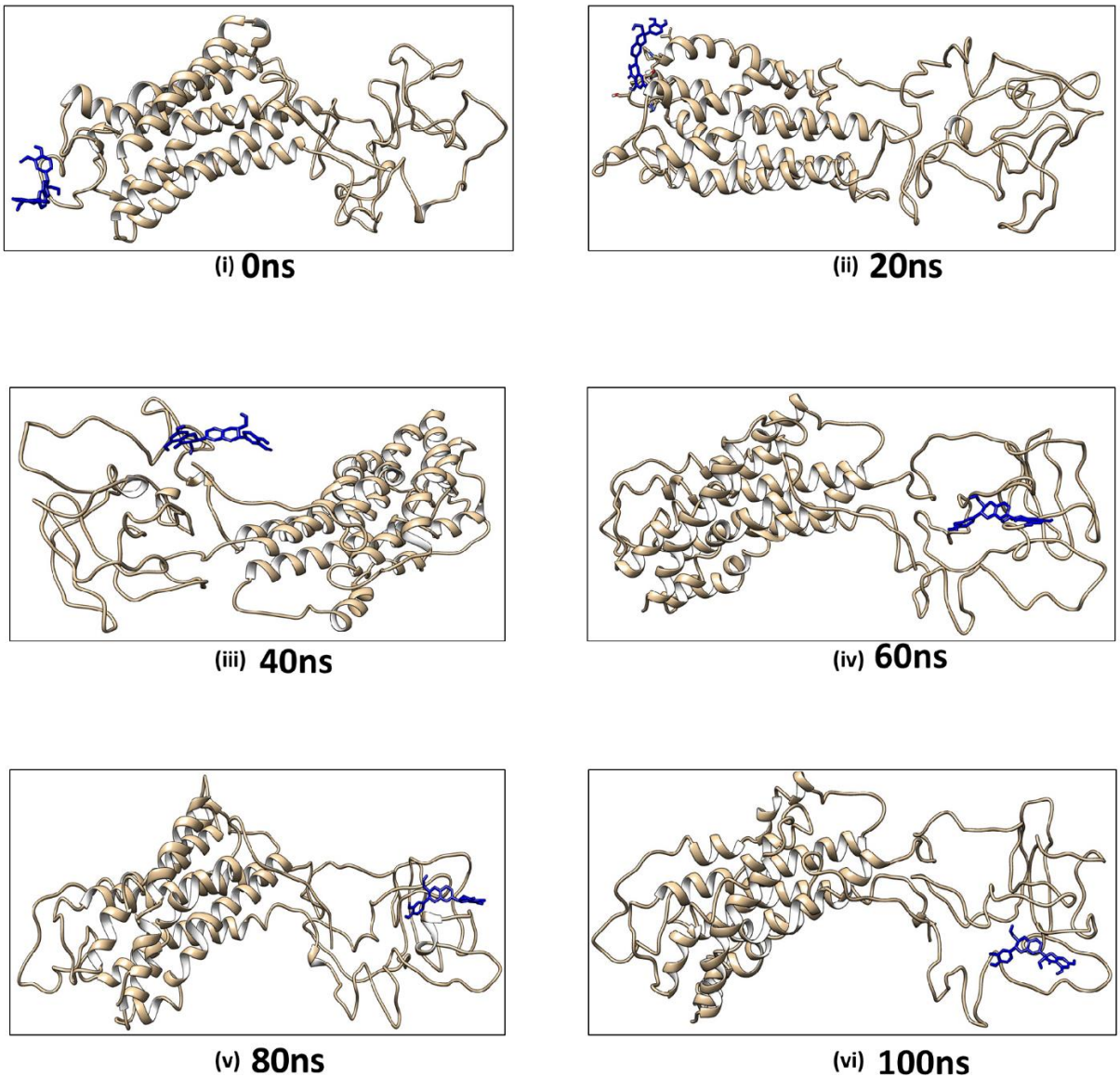

(A)

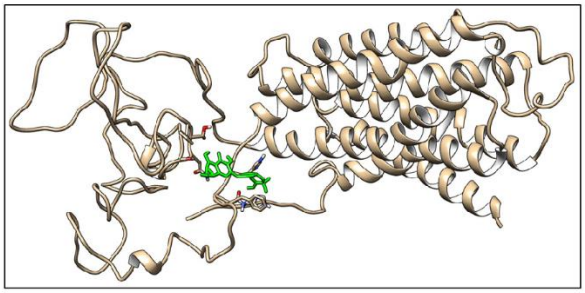

(i) 0ns

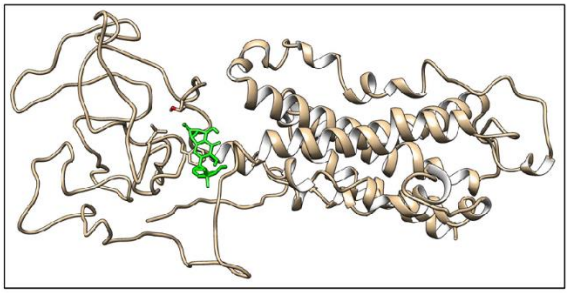

(ii) 20ns

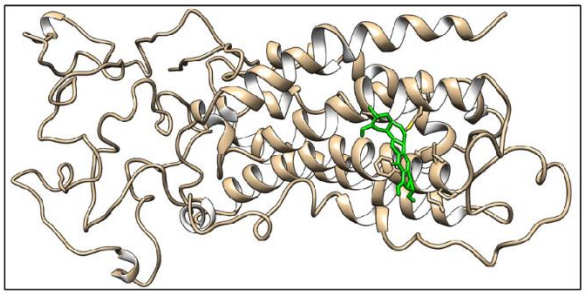

(iii) 40ns

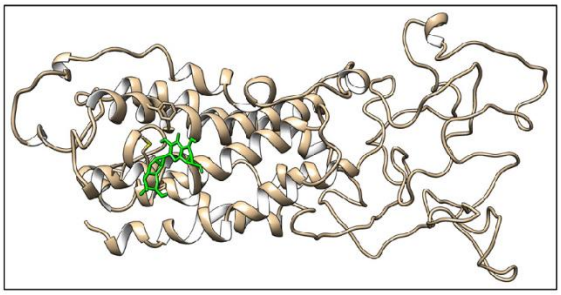

(iv) 60ns

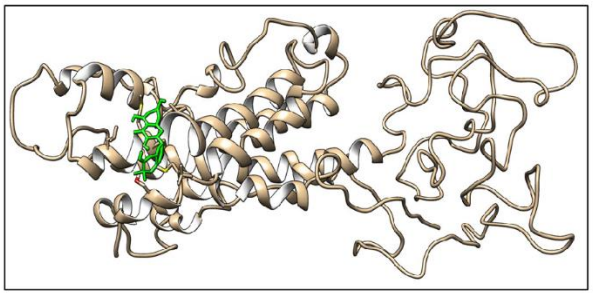

(v) 80ns

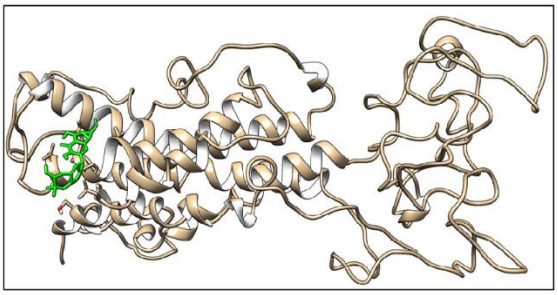

(vi) 100ns

(B)

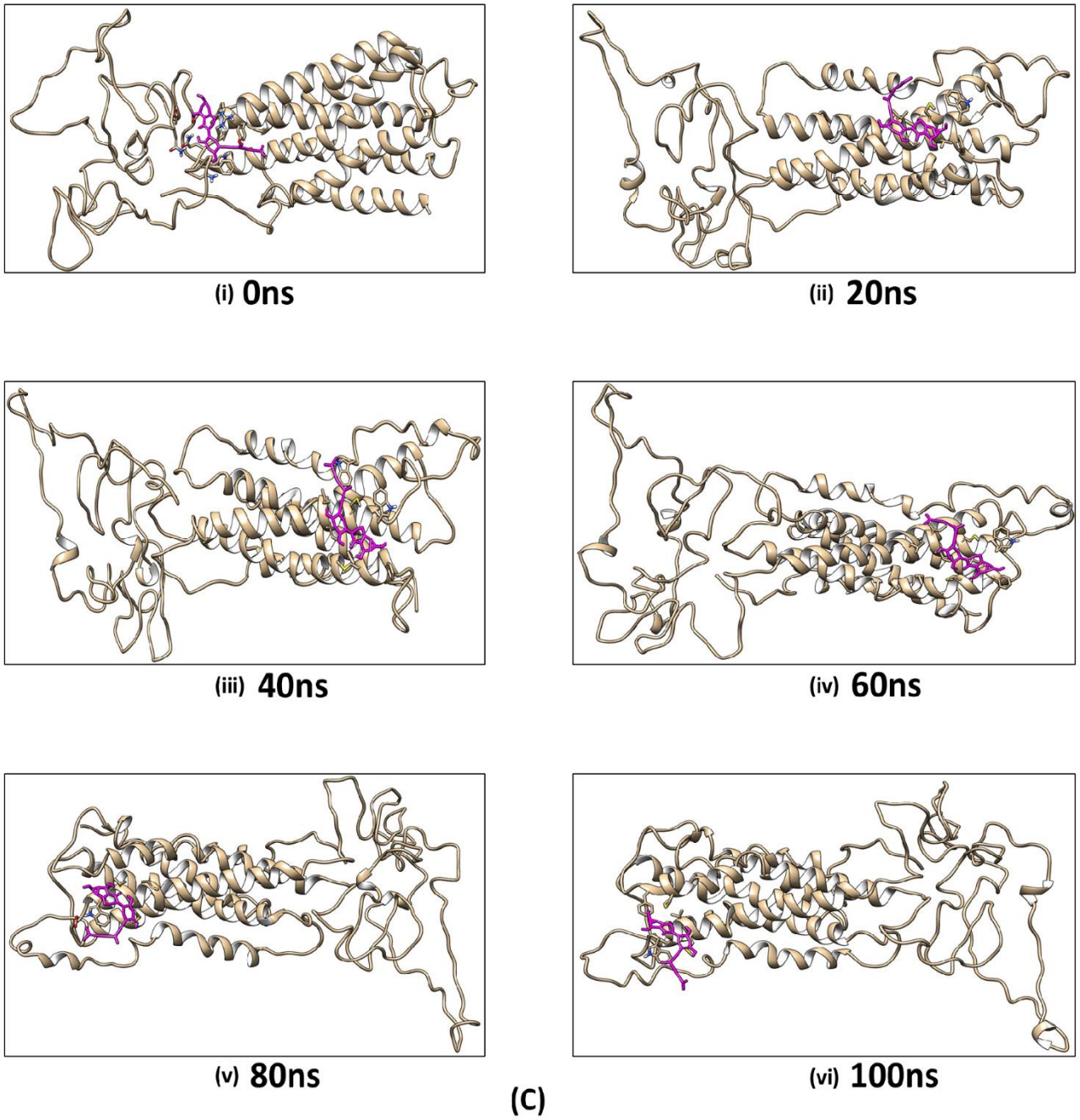

Figure 8: (A), (B) and (C) Shows conformation of lead compounds at different time intervals(ns) of selected compound silymarin (blue), glycyrrhiza (green) and kenusanone A (pink) respectively

5.8. MM-PBSA Simulation:

The MM-PBSA method was used to determine the binding free energy of all simulated complexes, thereby confirming their binding affinities. The binding free energies were computed using the data from the last 5 nanoseconds of the molecular dynamics' simulation trajectories. The MM-PBSA method was used to determine the binding free energy of all simulated complexes, thereby confirming their binding affinities. **Figure 9** provides comprehensive data on the specific values of van der Waals, electrostatic, polar solvation, solvation energy terms, molecular mechanics terms, nonpolar solvation and overall binding free energies.

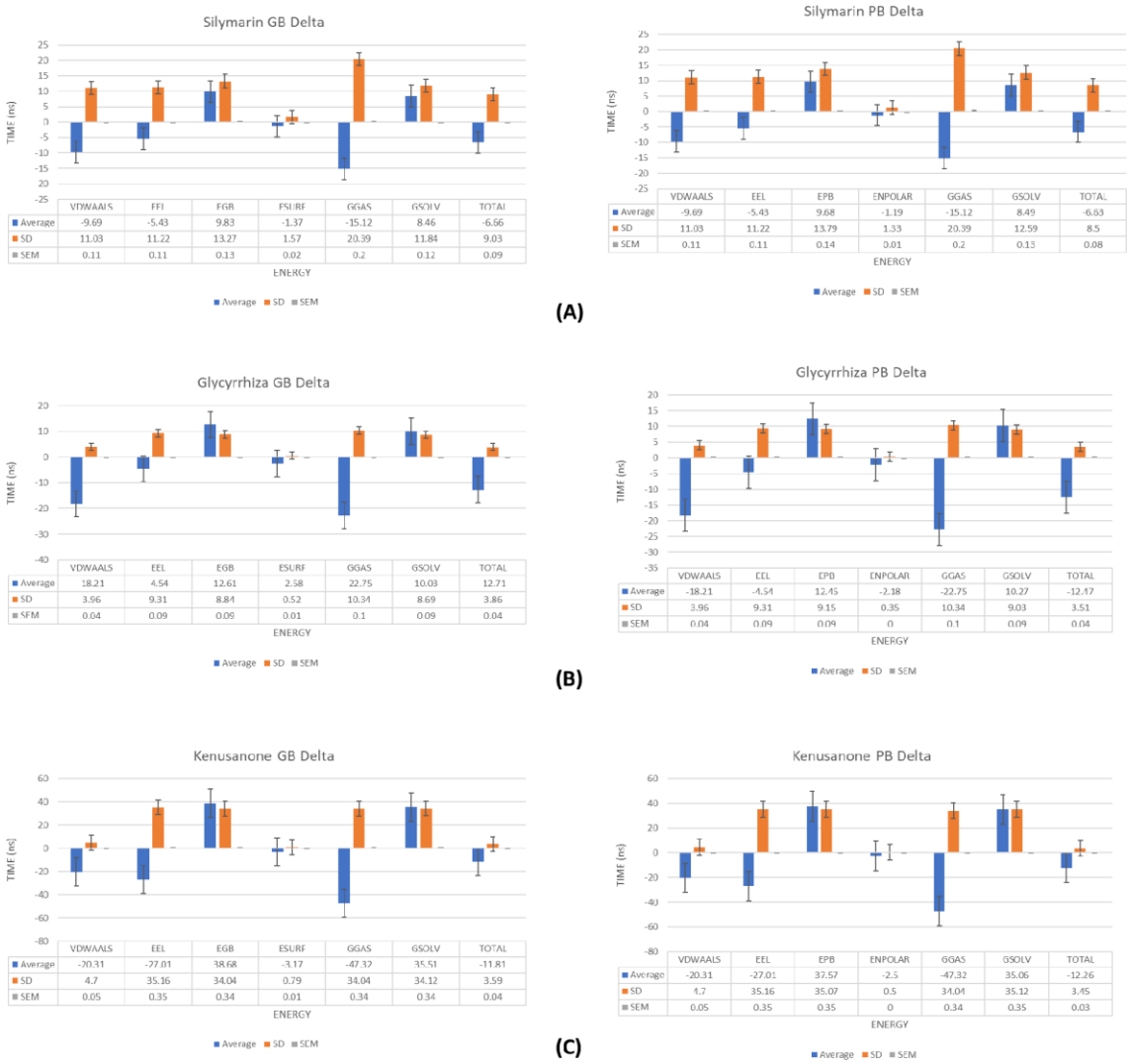

Figure 9: Binding energy on MM-PBSA calculation for the complexes along with standard error. (A), (B) and (C) Shows lead compounds silymarin, glycyrrhiza and kenusanone A respectively

5.9. Density Functional Theory:

The key compounds were subjected to optimisation using the Density Functional Theory (DFT) approach, employing the B3LYP functional and a 6-311G++(d,p) basis set. This optimisation facilitates assessing the molecule's interactions with other species by analysing its frontier molecular orbitals (FMO). More precisely, the analysis focuses on the lowest unoccupied molecular orbital (LUMO) and the highest occupied molecular orbital (HOMO). The HOMO functions as a nucleophile, donating electrons, while the LUMO acts as an electrophile, accepting electrons. Assessing the stability of a molecule involves evaluating FMOs by determining the energy difference between the HOMO and LUMO states. **Figure 10** shows the molecular orbitals of the HOMO LUMO for compounds silymarin and kenusanone.

Molecular electrostatic potential (MEP) analysis assesses the properties of a lead molecule by considering its shape, size, and electrostatic potential. The method employs colour gradients to represent the molecule's potential. MEP maps depict nucleophilic regions in blue and electrophilic regions in red. Intermediate colours are used to represent different potentials. The presence of red areas indicates regions with an abundance of electrons, while blue areas indicate regions with a scarcity of electrons, thereby indicating the polarisation of the molecule. This analysis identifies specific sites within a molecule that are prone to reacting with nucleophilic or electrophilic species. It helps in comprehending the molecule's stability, reactivity, and tendencies to interact with other substances. **Figure 10** A(i) and B(i) shows the molecular electrostatic potential.

Atomic Mulliken charges play an important part in quantum chemical calculations as they have a significant impact on various properties such as polarizability, vibrational spectra, dipole moment, and electronic structure. They disclose the distribution of charges in pairs of donors and acceptors during processes of charge transfer. The distribution of electric charge has a significant effect on the vibrational spectra of a molecule and indicates charge delocalization, crucial for understanding the molecule's reactivity and stability. **Figure 10** A(ii) and B(ii) shows the mulliken atomic charge distribution of the lead compounds.

(A) (B)

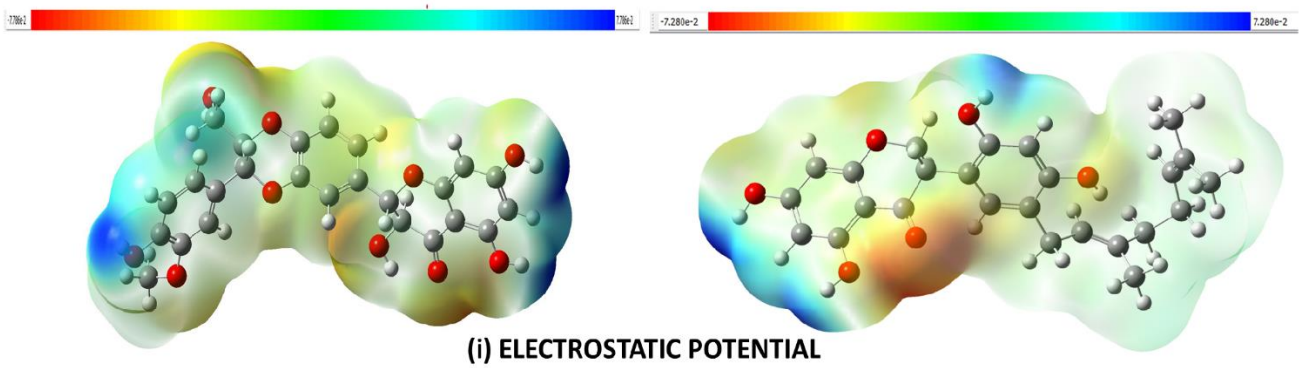

(i) ELECTROSTATIC POTENTIAL

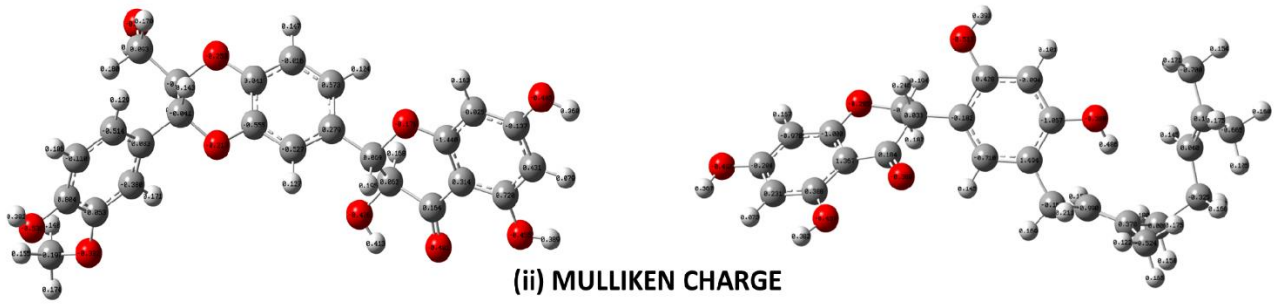

(ii) MULLIKEN CHARGE

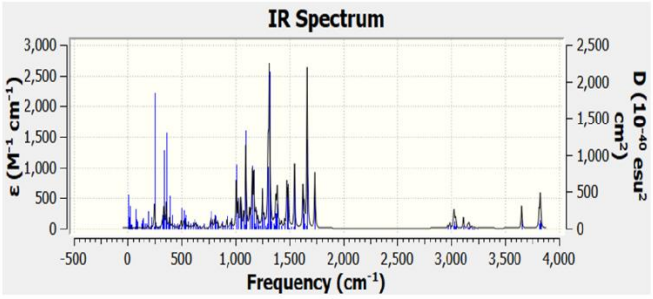

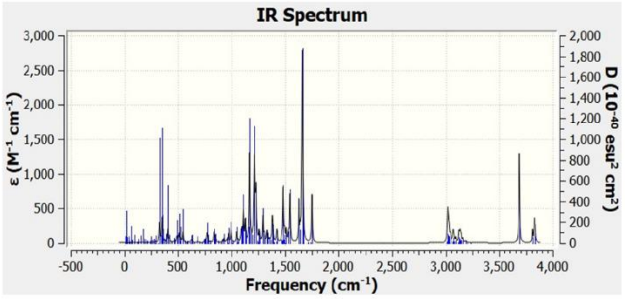

(iii) FREQUENCY SPECTRA

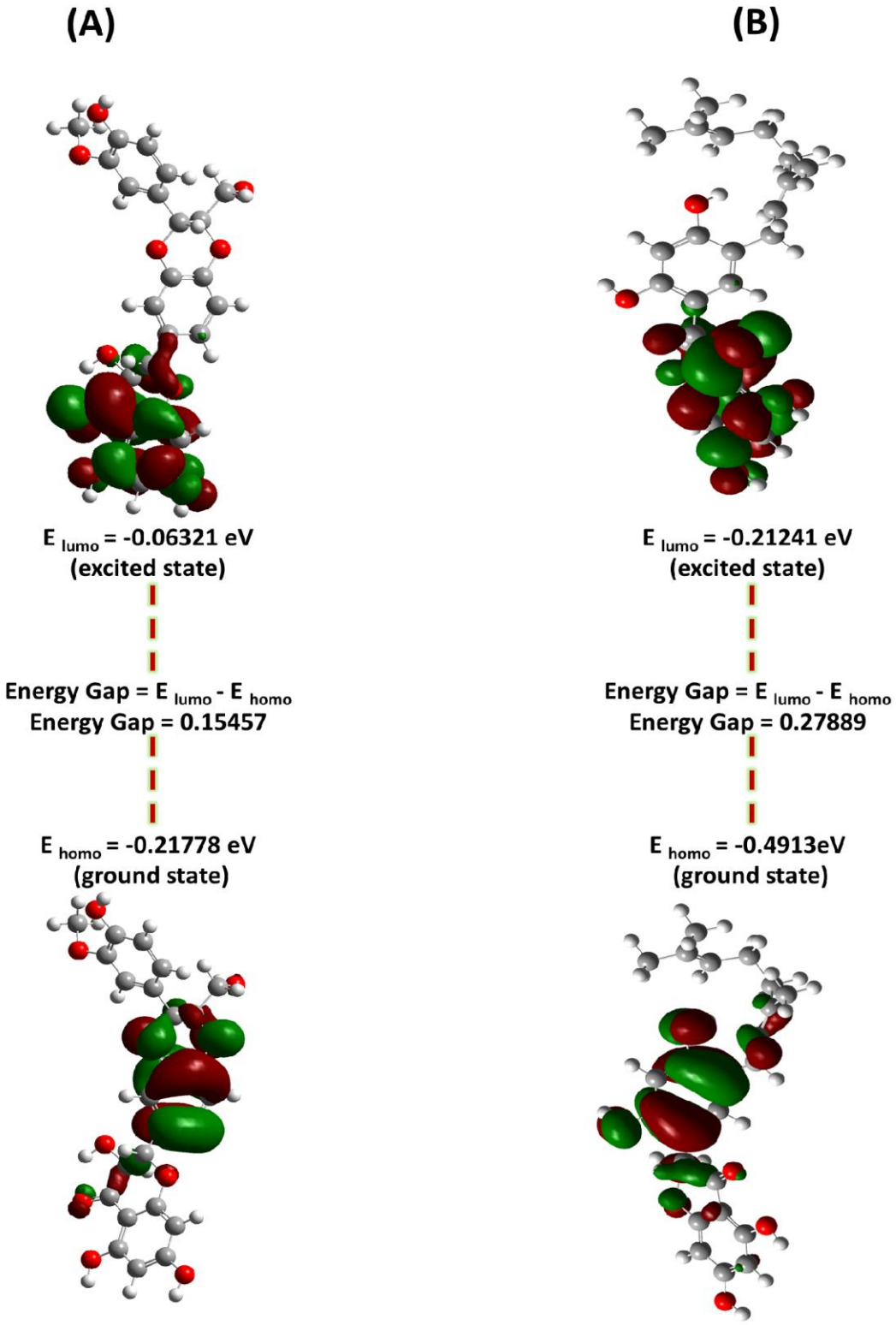

Figure 10: Depicts molecular electrostatic potential, mulliken atomic charge distribution, frequency spectra, and energy band gap between LUMO and HOMO of the lead molecules (A) silymarin and (B) kenusanone

CHAPTER 6 DISCUSSIONS

Most of the available anti-histamine interventions for the treatment of allergic reactions are a double-edged sword. As the medication offers signs of relief but the frequent use might hinder the immune system's ability to develop natural tolerance. Also, drowsiness and sedation are the biggest side effect in the first-generation antihistamine, meanwhile, the second generation has a lower propensity to cross the blood-brain barrier which leads to the minimization of sedation but still causes other side effects such as urinary retention, dry mouth or dizziness. The prolonged use of antihistamines can increase the risk of glioma i.e. a cancerous brain tumour, in individuals with a history of taking antihistamines(Scheurer et al., 2008). This study investigates the potential of novel compounds as an anti-allergic agent targeting human histamine H1 receptors. The utilisation of natural compounds in the treatment of intricate ailments can be traced back to ancient times when many therapeutic options existed. Because of advancements in scientific technology, our knowledge and utilisation of natural compounds for therapeutic purposes are constantly progressing.

Out of 100 compounds showing anti-allergic activity, only 10 lead compounds were selected based on molecular docking parameters i.e. docking score which was less than -7.5 Kcal/mol. The docked complexes were analysed in BIOVIA Discovery studio to check the interactions and bond type between the protein and selected lead compounds. The conventional hydrogen bond in the interaction analyses makes the complex more stable and rigid. Then, molecular filters and ADMET evaluation were used to predict the physicochemical parameters among the compounds. Out of 10 only 3 compounds were selected as they pass all the parameters of a drug candidate.

To assess the overall stability of each predicted lead compound, Molecular Dynamic Simulations were conducted. It is a highly effective method of predicting the behavior of macromolecules before and after they bind to the ligand. Additionally, the simulated data were utilised to compute the binding free energy of each compound as it progressed over time subsequently. The amino acid residues of the human histamine H1 receptor contribute to the stabilisation of the protein-ligand complex. The RMSD analysis indicated that all systems achieved stabilisation after 100 ns, indicating a substantial interaction between the predicted lead compounds and the receptor. Hence, the last 100 nanosecond trajectories were employed to examine additional parameters including RMSF (Root Mean Square Fluctuation), Rg (Radius of Gyration), RMSD (Root mean square Deviation), SASA (Solvent Accessible

Surface Area), H-bonds (Hydrogen Bonds), and PCA (Principal Component Analysis) to ascertain the characteristics of each compound. The analysis determined that the binding of the ligand alters both the conformation and dynamics of the protein, which are necessary for inhibition.

Further investigation of the affinity of the natural compounds for the protein receptor was carried out using the MM-PBSA method to calculate the binding free energy and residual binding energy. The data on the protein-ligand complex's binding free energy was obtained from molecular dynamics (MD) simulations. The ligand binding affinity, directly correlated with the ligand potency, was determined by measuring the strength of the binding interaction between each compound and the receptor. In addition, the free energy of the favourable reactions is negative. Thus, reducing the binding energy increases the interactions, whereas the strong binding affinity of the protein-ligand complexes is associated with a decrease in binding free energy. Based on MDS and MMPBSA calculations, it was concluded that silymarin and kenusanone A were the selected predicted compounds that target the Human histamine H1 Receptor i.e. 3RZE.

From the DFT evaluation, the energy gap computed in silymarin was ΔE=0.15457 eV and in kenusanone A is ΔE=0.27889 eV. The mulliken charge distribution analysis was performed which ranges in silymarin between -1.440 to 0.804 and in kenusanone between -1.067 to 1.494. Therefore, the findings in the present investigation are informative in developing antihistamine drugs with minimization of toxicity and good biocompatibility against the human target histamine H_1 receptor.

CHAPTER 7 CONCLUSIONS

A number of in silico studies and computational methods were employed in the present study to find new and potent compound that can act as an antihistamine targeting the human Histamine H_1 receptor i.e. 3RZE. This study predicts that silymarin and kenusanone A possess the potential to be formulated as a drug candidate with antihistamine properties targeting the histamine H1 receptor. By conducting a thorough examination that included molecular docking, ADMET evaluation, and molecular dynamic simulations, it was found that these compounds exhibited notable binding affinity, stability, and favourable physicochemical properties. The diminished affinity of binding and enduring protein-ligand interactions indicates their effectiveness in suppressing allergic responses while minimising adverse effects. The findings provide valuable insights that can be used to develop antihistamine drugs that are safer and more effective. These drugs can make use of the therapeutic potential of natural compounds. Further investigation should prioritise thorough in vitro and in vivo examinations to confirm the effectiveness and safety of silymarin and kenusanone A in treating allergies. Additionally, detailed evaluations of the pharmacokinetics, pharmacodynamics, and toxicology should be conducted. By making structural changes and conducting SAR (structure-activity relationship) studies, it is possible to improve the ability of these compounds to bind to specific targets and increase their selectivity. However, it is ultimately the results of clinical trials that will determine their potential as therapeutic agents in humans. Mechanistic investigations will clarify the molecular interactions, while comparative analyses with current antihistamines will emphasise their benefits. Exploring the use of combination therapies and conducting extensive studies on their long-term effectiveness will help solidify their practical value in clinical settings. Furthermore, the advancement of optimised drug formulations will ensure effective delivery and patient compliance, ultimately driving these compounds towards becoming viable antihistamine medications.

Agu, P. C., Afiukwa, C. A., Orji, O. U., Ezeh, E. M., Ofoke, I. H., Ogbu, C. O., Ugwuja, E. I., & Aja, P. M. (2023). Molecular docking as a tool for the discovery of molecular targets of nutraceuticals in diseases management. *Scientific Reports*, *13*(1), 13398. https://doi.org/10.1038/s41598-023-40160-2

Akamine, Y., Yasui-Furukori, N., & Uno, T. (2019). Drug-Drug Interactions of P-gp Substrates Unrelated to CYP Metabolism. *Current Drug Metabolism*, *20*(2), 124–129. https://doi.org/10.2174/1389200219666181003142036

Andorf, S., Borres, M. P., Block, W., Tupa, D., Bollyky, J. B., Sampath, V., Elizur, A., Lidholm, J., Jones, J. E., Galli, S. J., Chinthrajah, R. S., & Nadeau, K. C. (2017). Association of Clinical Reactivity with Sensitization to Allergen Components in Multifood-Allergic Children. *The Journal of Allergy and Clinical Immunology: In Practice*, *5*(5), 1325-1334.e4. https://doi.org/10.1016/j.jaip.2017.01.016

Antonijoan, R., Coimbra, J., García-Gea, C., Puntes, M., Gich, I., Campo, C., Valiente, R., & Labeaga, L. (2017). Comparative efficacy of bilastine, desloratadine and rupatadine in the suppression of wheal and flare response induced by intradermal histamine in healthy volunteers. *Current Medical Research and Opinion*, *33*(1), 129–136. https://doi.org/10.1080/03007995.2016.1240665

Baell, J. B., & Nissink, J. W. M. (2018). Seven Year Itch: Pan-Assay Interference Compounds (PAINS) in 2017—Utility and Limitations. *ACS Chemical Biology*, *13*(1), 36–44. https://doi.org/10.1021/acschembio.7b00903

Baltes, E., Coupez, R., Giezek, H., Voss, G., Meyerhoff, C., & Benedetti, M. S. (2001). Absorption and disposition of levocetirizine, the eutomer of cetirizine, administered alone or as cetirizine to healthy volunteers. *Fundamental & Clinical Pharmacology*, *15*(4), 269–277. https://doi.org/10.1046/j.1472-8206.2001.00035.x

Banjare, P., Sarthi, A. S., Singh, J., & Roy, P. P. (2020). *In-Silico Approaches in Drug Discovery and Design of Anti-Allergic Agents* (pp. 94–132). https://doi.org/10.2174/9789811428395120040006

Barbanoj, M. J., García-Gea, C., Morte, A., Izquierdo, I., Pérez, I., & Jané, F. (2004). Central and Peripheral Evaluation of Rupatadine, a New Antihistamine/Platelet-Activating Factor Antagonist, at Different Doses in Healthy Volunteers. *Neuropsychobiology*, *50*(4), 311–321. https://doi.org/10.1159/000080959

Chen, C. (2008). Physicochemical, Pharmacological and Pharmacokinetic Properties of the Zwitterionic Antihistamines Cetirizine and Levocetirizine. *Current Medicinal Chemistry*, *15*(21), 2173–2191. https://doi.org/10.2174/092986708785747625

Estelle, F., Simons, R., & Simons, K. J. (n.d.). *H 1 Antihistamines Current Status and Future Directions*.

Hadda, T. Ben, Rastija, V., AlMalki, F., Titi, A., Touzani, R., Mabkhot, Y. N., Khalid, S., Zarrouk, A., & Siddiqui, B. S. (2021). Petra/Osiris/Molinspiration and Molecular Docking Analyses of 3-Hydroxy-Indolin-2-one Derivatives as Potential Antiviral Agents. *Current Computer-Aided Drug Design*, *17*(1), 123–133. https://doi.org/10.2174/1573409916666191226110029

Horak, F., Zieglmayer, P., Zieglmayer, R., & Lemell, P. (2010). The effects of bilastine compared with cetirizine, fexofenadine, and placebo on allergen-induced nasal and ocular symptoms in patients exposed to aeroallergen in the Vienna Challenge Chamber. *Inflammation Research*, *59*(5), 391–398. https://doi.org/10.1007/s00011-009-0117-4

Hu, G., Li, X., Zhang, J., Zhang, L., Qi, J., & Yu, B. (2021). An integrated strategy for the identification and screening of anti-allergy components from natural products based on calcium fluctuations and cell extraction coupled with HPLC–Q–TOF–MS. *Analytical and Bioanalytical Chemistry*, *413*(25), 6253–6266. https://doi.org/10.1007/s00216-021-03580-5

Khan, T., Dixit, S., Ahmad, R., Raza, S., Azad, I., Joshi, S., & Khan, A. R. (2017). Molecular docking, PASS analysis, bioactivity score prediction, synthesis, characterization and biological activity evaluation of a functionalized 2-butanone thiosemicarbazone ligand and its complexes. *Journal of Chemical Biology*, *10*(3), 91–104. https://doi.org/10.1007/s12154-017-0167-y

Kim, S., Chen, J., Cheng, T., Gindulyte, A., He, J., He, S., Li, Q., Shoemaker, B. A., Thiessen, P. A., Yu, B., Zaslavsky, L., Zhang, J., & Bolton, E. E. (2023). PubChem 2023 update. *Nucleic Acids Research*, *51*(D1), D1373–D1380. https://doi.org/10.1093/nar/gkac956

O'Mahony, L., Akdis, M., & Akdis, C. A. (2011). Regulation of the immune response and inflammation by histamine and histamine receptors. *Journal of Allergy and Clinical Immunology*, *128*(6), 1153–1162. https://doi.org/10.1016/j.jaci.2011.06.051

Pajno, G. B., Fernandez-Rivas, M., Arasi, S., Roberts, G., Akdis, C. A., Alvaro-Lozano, M., Beyer, K., Bindslev-Jensen, C., Burks, W., Ebisawa, M., Eigenmann, P., Knol, E., Nadeau, K. C., Poulsen, L. K., van Ree, R., Santos, A. F., du Toit, G., Dhami, S.,

Nurmatov, U., … Muraro, A. (2018). <scp>EAACI</scp> Guidelines on allergen immunotherapy: IgE-mediated food allergy. *Allergy*, *73*(4), 799–815. https://doi.org/10.1111/all.13319

Potter, P., Mitha, E., Barkai, L., Mezei, G., Santamaría, E., Izquierdo, I., & Maurer, M. (2016). Rupatadine is effective in the treatment of chronic spontaneous urticaria in children aged 2–11 years. *Pediatric Allergy and Immunology*, *27*(1), 55–61. https://doi.org/10.1111/pai.12460

Sabban, S. S. (2021). Computationally grafting an IgE epitope onto a scaffold: Implications for a pan anti-allergy vaccine design. *Computational and Structural Biotechnology Journal*, *19*, 4738–4750. https://doi.org/10.1016/j.csbj.2021.08.012

Sabe, V. T., Ntombela, T., Jhamba, L. A., Maguire, G. E. M., Govender, T., Naicker, T., & Kruger, H. G. (2021). Current trends in computer aided drug design and a highlight of drugs discovered via computational techniques: A review. *European Journal of Medicinal Chemistry*, *224*, 113705. https://doi.org/10.1016/j.ejmech.2021.113705

Scheurer, M. E., El-Zein, R., Thompson, P. A., Aldape, K. D., Levin, V. A., Gilbert, M. R., Weinberg, J. S., & Bondy, M. L. (2008). Long-term Anti-inflammatory and Antihistamine Medication Use and Adult Glioma Risk. *Cancer Epidemiology, Biomarkers & Prevention*, *17*(5), 1277–1281.

Schrödinger, L., & DeLano, W. (2020). *PyMOL*.

Shimamura, T., Shiroishi, M., Weyand, S., Tsujimoto, H., Winter, G., Katritch, V., Abagyan, R., Cherezov, V., Liu, W., Han, G. W., Kobayashi, T., Stevens, R. C., & Iwata, S. (2011). Structure of the human histamine H1 receptor complex with doxepin. *Nature*, *475*(7354), 65–70. https://doi.org/10.1038/nature10236

Simons, F. E. R. (2004). Advances in H $_1$ -Antihistamines. *New England Journal of Medicine*, *351*(21), 2203–2217. https://doi.org/10.1056/NEJMra033121

Tenn, M. W., Steacy, L. M., Ng, C. C., & Ellis, A. K. (2018). Onset of action for loratadine tablets for the symptomatic control of seasonal allergic rhinitis in adults challenged with ragweed pollen in the Environmental Exposure Unit: a post hoc analysis of total symptom score. *Allergy, Asthma & Clinical Immunology*, *14*(1), 5. https://doi.org/10.1186/s13223-017-0227-4

Waterhouse, A., Bertoni, M., Bienert, S., Studer, G., Tauriello, G., Gumienny, R., Heer, F. T., de Beer, T. A. P., Rempfer, C., Bordoli, L., Lepore, R., & Schwede, T. (2018). SWISS-MODEL: homology modelling of protein structures and complexes. *Nucleic Acids Research*, *46*(W1), W296–W303. https://doi.org/10.1093/nar/gky427

Wood, S. G., John, B. A., Chasseaud, L. F., Yeh, J., & Chung, M. (1987). The metabolism and pharmacokinetics of 14C-cetirizine in humans. *Annals of Allergy*, *59*(6 Pt 2), 31–34.

Wu, K. G., Li, T. H., Wang, T. Y., Hsu, C. L., & Chen, C. J. (2012). A Comparative Study of Loratadine Syrup and Cyproheptadine HCL Solution for Treating Perennial Allergic Rhinitis in Taiwanese Children Aged 2–12 Years. *International Journal of Immunopathology and Pharmacology*, *25*(1), 231–237. https://doi.org/10.1177/039463201202500125

Xiong, G., Wu, Z., Yi, J., Fu, L., Yang, Z., Hsieh, C., Yin, M., Zeng, X., Wu, C., Lu, A., Chen, X., Hou, T., & Cao, D. (2021). ADMETlab 2.0: an integrated online platform for accurate and comprehensive predictions of ADMET properties. *Nucleic Acids Research*, *49*(W1), W5–W14. https://doi.org/10.1093/nar/gkab255

Zulfiqar, H., Masoud, M. S., Yang, H., Han, S.-G., Wu, C.-Y., & Lin, H. (2021). Screening of Prospective Plant Compounds as H1R and CL1R Inhibitors and Its Antiallergic Efficacy through Molecular Docking Approach. *Computational and Mathematical Methods in Medicine*, *2021*, 1–9. https://doi.org/10.1155/2021/6683407

DrillBit

The Report is Generated by DrillBit Plagiarism Detection Software

Submission Information

Author Name	Shivangi Jain
Title	Natural Compounds Targeting Human Histamine H 1 Receptor For Anti-Allergic Therapy
Paper/Submission ID	2184593
Submitted by	atul.upadhyay@thapar.edu
Submission Date	2024-07-30 15:40:30
Total Pages, Total Words	24, 7905
Document type	Thesis

Result Information

Similarity **16 %**

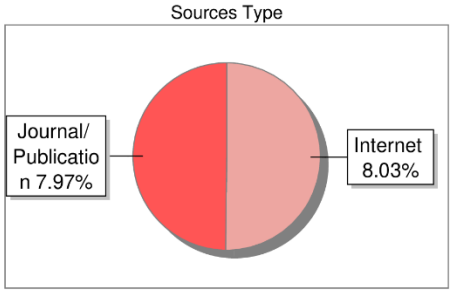

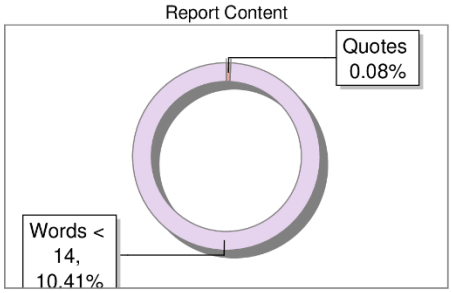

Exclude Information

Quotes	Not Excluded
References/Bibliography	Not Excluded
Source: Excluded < 14 Words	Not Excluded
Excluded Source	**0 %**
Excluded Phrases	Not Excluded

Database Selection

Language	English
Student Papers	Yes
Journals & publishers	Yes
Internet or Web	Yes
Institution Repository	Yes

A Unique QR Code use to View/Download/Share Pdf File